Table 2. *Accuracy of fit to a three-parameter logarithmic function*

Dog	Right Ventricle		Left Ventricle	
	r^2	SEE	r^2	SEE
	Normal heart			
1	0.99	5.3	0.98	6.9
2	0.96	7.2	0.89	11.6
3	0.96	11.4	0.96	10.5
4	0.96	6.9	0.99	4.0
5	0.96	6.6	0.97	6.0
6	0.97	7.7	0.99	4.7
Mean ± SD	0.97	7.5 ± 2.1	0.96	7.3 ± 3.1
	Left heart failure			
1	0.96	2.2	0.89	4.5
2	0.98	2.0	0.97	2.4
3	0.99	1.9	0.99	1.8
4	0.96	2.1	0.97	1.9
5	0.73	2.9	0.84	2.7
6	0.92	2.7	0.94	2.3
Mean ± SD	0.92	2.3 ± 0.4	0.93	2.6 ± 1.0

their distributions (see APPENDIX), the flatness of the surface would depend on how constant the vascular resistance and compliance remained, irrespective of loading conditions. Drees and Rothe (9) found that compliance of the total vasculature was remarkably constant from 5 to 25 mmHg of mean circulatory filling pressure. Grodins et al. (13) reported a fairly linear relation between the systemic venous return and P_{RA} from 5 to 20 mmHg. These reports and many other studies (8, 18, 26) demonstrated the constant nature of vascular compliance and resistance in physiologically normal pressure ranges. However, it is uncertain whether the parameters remain constant when the pressure range is further expanded to include lower or higher values (1, 7, 16). The venous return curve of Guyton et al. (16) reaches a maximum value and remains on a plateau at all P_{RA} less than −2 mmHg. Although we did not observe such a curvature of the venous return surface, it is conceivable that the surface might not be flat if we were to impose extreme experimental conditions. Nevertheless, it is fair to say that the venous return surface is reasonably flat within a physiologically normal range of pressures.

A standard set of parameters for the venous return surface enabled us to predict CO and atrial pressures for changes in stressed volume, if the CO curve is defined. The lack of variability of three parameters (W, G_S, and G_P) among animals is the underlying reason for this observation. As indicated in the APPENDIX, these parameters are complex functions of vascular resistance and compliance and their distributions. Therefore, the lack of variability of these parameters reflects the lack of variability of vascular resistance and compliance and their distributions among animals. Indeed, reported values for total compliance and resistance for venous return of the pulmonary and systemic circulation were very close (19, 26). The values for W, G_S, and G_P estimated by combining data of Lee and Goldman (19) and data of Shoukas (26) are 0.131 min, 14.56 $ml \cdot min^{-1} \cdot mmHg^{-1} \cdot kg^{-1}$, and 2.39 $ml \cdot min^{-1} \cdot mmHg^{-1} \cdot kg^{-1}$, respectively (see APPENDIX), which are reasonably close to the standard values of the venous return surface parameters obtained in this study. Thus the parameter values obtained in our study are not specific for our experiment but are generally reproducible.

Integrated CO Curve

We measured the CO curves of both ventricles by changing the stressed blood volume (25, 28). The mean slopes of the right and left CO curves under normal cardiac conditions were 55.6 ± 18.7 and 27.2 ± 12.3 $ml \cdot min^{-1} \cdot mmHg^{-1} \cdot kg^{-1}$, respectively, which are reasonably close to those found in the previous study (28).

A three-parameter logarithmic function approximated the CO curves well. According to the framework of ventricular-arterial coupling using the volume-elastance concept, CO, or stroke volume under a constant contractility, arterial resistance and heart rate depend linearly on end-diastolic volume (24, 29). Therefore, the logarithmic relation between CO and atrial pressure would be a manifestation of the logarithmic relation

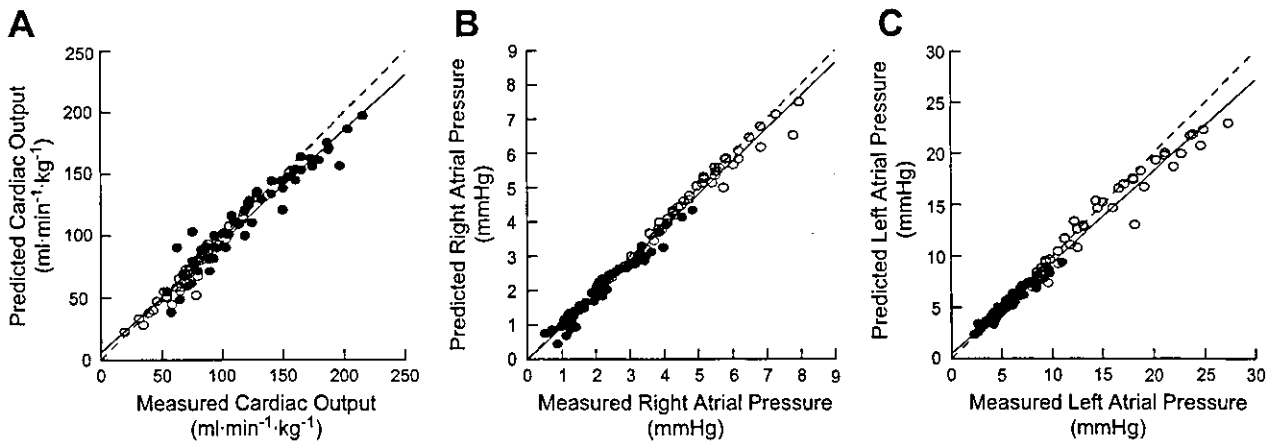

Fig. 8. Relations between values predicted and actually measured for CO (*A*), P_{RA} (*B*), and P_{LA} (*C*) for 104 steps pooled over 12 output curves. ●, Normal cardiac function; ○, left heart failure; dashed lines, lines of identity. Regression analysis (solid lines) revealed that predicted CO ($y = 0.90x + 5.6$, $n = 104$, $r^2 = 0.95$, SEE = 8.7 $ml \cdot min^{-1} \cdot kg^{-1}$), P_{RA} ($y = 0.96x$, $n = 104$, $r^2 = 0.98$, SEE = 0.2 mmHg), and P_{LA} ($y = 0.89x + 0.5$, $n = 104$, $r^2 = 0.98$, SEE = 0.8 mmHg) agreed reasonably well with measured values.

between end-diastolic volume and filling pressure. This is indeed reasonable, because the pressure-volume relation of the diastolic ventricle is known to be exponential; therefore, the volume-pressure relation should be the inverse of exponential, i.e., logarithmic (12).

Mechanical parameters such as ventricular systolic and diastolic elastance, heart rate, ventricular interdependence, and arterial resistance have been shown to affect CO (22, 24). To clarify therapeutic targets in the management of cardiac patients, it is crucial to relate those mechanical parameters to the CO curve, as we have done with the venous return surface. Modeling the CO curve on the basis of those parameters is clearly required in future studies.

Analysis of the Circulatory Equilibrium

The venous return surface, combined with the integrated CO curve in the three-dimensional diagram, enables us to make intuitive and in-depth analyses of the contribution of the individual system components to hemodynamics. Figure 9 illustrates the effect of left heart failure on circulatory equilibrium. Integrated CO curves, which were experimentally obtained from a dog under normal and left heart failure conditions, are superimposed on the standard venous return surface in Fig. 9*A*. Under the normal condition, the integrated CO curve intersects the surface at a CO of 115 ml·min^{-1}·kg^{-1}, with a P_{RA} of 2.5 mmHg and a P_{LA} of 4.1 mmHg. In contrast, left heart failure lessens the slope of the CO curve and diverts it toward the axis of P_{LA}. At the intersection of the standard surface and the CO curve under left heart failure, although the CO decreased (85 ml·min^{-1}·kg^{-1}), the increase in P_{LA} (9.3 mmHg) was modest. When the stressed blood volume is increased to simulate the baroreflex response (+8 ml/kg), the surface shifts upward (Fig. 9*B*). The intersection reached a new equilibrium point, where P_{LA} increased drastically (15.9 mmHg) with a slight increase in P_{RA} and a partial recovery of CO. Although this analysis is hypothetical, the graphical analysis represents the typical hemodynamics of left heart failure (2, 4, 10, 23, 35). Notwithstanding its simplicity, the framework for the venous return surface provides a very powerful tool for analysis of complicated hemodynamics in the clinical setting.

Comparison with Previous Studies of Cardiovascular Modeling

Many studies have modeled hemodynamics of the cardiovascular system (3–5, 20, 31, 33). The parallel circuit model of Caldini et al. (5) seems to be more appropriate than our serial model for an anatomically oriented analysis of hemodynamics within a single circulation, i.e., the analysis of blood redistribution between the splanchnic and nonsplanchnic circuits. Levy (20) simplified blood distribution between the arterial and venous compartments with a lumped serial model. Although these models could analyze hemodynamics within a single circulation, they were not intended to deal with blood redistribution between the systemic and the pulmonary circulation. In contrast, the two-compartment model of Guyton et al. (15) and the multiple-circuit model proposed by Sylvester et al. (31) can address this issue. These studies, however, went no further than a theoretical analysis and remain insufficient for clinical application. The two-compartment model of Guyton et al. is complicated. It fails to express venous return curves parametrically; consequently, neither the stressed blood volume nor the curve shifts in response to changes in stressed blood volume can be estimated (15). Sylvester et al. (31) integrated systemic and pulmonary venous return curves into a single curve and expressed it parametrically. However, extensive experimental validations of the model are needed. In addition, because the pressure axis of their integrated venous return curve was the weighted average of P_{RA} and P_{LA}, we were unable to uniquely determine their individual values from the equilibrium point in their diagram.

There have been serious debates among cardiovascular physiologists regarding cause-effect relations between CO/venous return and atrial pressure, i.e., which variable determines the others? Brengelmann (3), Levy (20), and Tyberg (33) argued that as CO increases, the venous reservoir is depleted (i.e., blood is translocated from the veins to the arteries), and, therefore, venous pressure (i.e., atrial pressure) decreases. In the heart, atrial pressure determines CO according to the Frank-Starling mechanism. In contrast, in response to the work of Levy, Guyton (14) commented that he considered CO and atrial pressures to be the effects, or dependent variables. Blood volume and the mechanical properties of the heart and vasculature, such as heart rate, ventricular contractility,

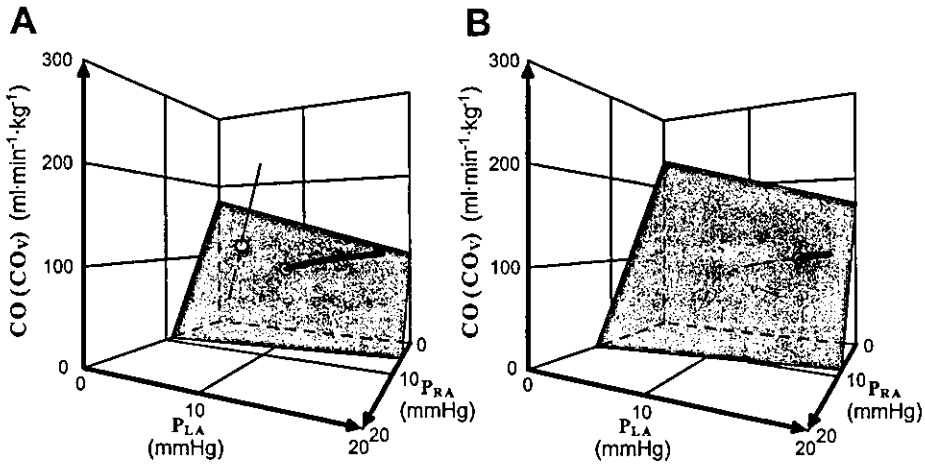

Fig. 9. *A*: integrated CO curves under normal cardiac conditions (thin solid line) and left heart failure condition (thick solid line) superimposed with the standard venous return surface with control stressed blood volume. ○, Intersection of curves and standard venous return surface. Compared with normal hemodynamics (P_{RA} = 2.5 mmHg, P_{LA} = 4.1 mmHg, CO = 115 ml·min^{-1}·kg^{-1}), CO decreased and both P_{LA} and P_{RA} increased under left heart failure (P_{RA} = 3.1 mmHg, P_{LA} = 9.3 mmHg, and CO = 85 ml·min^{-1}·kg^{-1}). *B*: integrated CO curve under left heart failure condition (thick solid line) superimposed with the standard venous return surface with increased stressed blood volume (8 ml/kg). At the new equilibrium point, P_{LA} (15.9 mmHg) drastically increased with a slight increase in P_{RA} (4.0 mmHg) and partial recovery of CO (106 ml·min^{-1}·kg^{-1}).

and vascular resistance, are the cause. The CO curve or venous return curve discloses those properties through the relation between the flow and atrial pressures. As we demonstrated in *Eq. 1*, under a given stressed volume, venous return/CO and atrial pressure have a linear relation. In other words, once venous return is determined, atrial pressure is automatically determined and vice versa. Therefore, our framework is consistent with Guyton's comment on the work of Levy. As far as the prediction of hemodynamics is concerned, however, the difference between their interpretations and ours does not impact the result of this study, because we are able to obtain the same equilibrium point with either interpretation (14, 20).

Application of This Framework

Accurate predictions of CO and filling pressures after therapeutic interventions are vital in the management of heart failure, as suggested by the classification of Forrester (10) and other previous studies (11, 21). Although the Swan-Ganz catheter allows us to estimate CO and filling pressures, such devices do not allow us to estimate the venous return curve or mean circulatory filling pressure (6). In contrast, because the parameter values of the venous return surface were invariable among animals, it is conceivable that the same standard values obtained from this investigation might be used for patients. If this is the case, for given values of CO, P_{LA}, and P_{RA}, all of which can be easily obtained by Swan-Ganz catheters, we can uniquely define the venous return surface and estimate stressed blood volume of patients without the need to perform total heart bypass (6). The clinical usefulness of knowing the venous return surface would be markedly increased if the integrated CO curve could be estimated. This would enable accurate prediction of the CO, P_{RA}, and P_{LA} in response to various therapeutic interventions, which induce changes in loading condition, or changes in the pumping ability of the heart, i.e., changes in CO curves. These should help optimize hemodynamic management and improve patient prognosis (10, 21).

Limitations

In this investigation, we isolated baroreceptors and fixed the autonomic tone. This was necessary, because the baroreflex alters the CO curve and venous return surface through its effects on stressed blood volume, vascular resistance, heart rate, and cardiac contractility (9, 24, 27). How changes in autonomic tone under the closed-loop condition affect the CO curve and venous return surface remains to be investigated.

We assumed that there is no fluid shift between the intravascular and extravascular space and that the volume perturbations exclusively changed the stressed blood volume. We assumed that the changes of cardiac volume and volume shifts between the heart and vasculatures are rather small. However, this may not be the case if the ventricles are extremely compliant, as in those with extensive remodeling (32). In such cases, the volume shifts between the heart and the vasculatures become significant. Further studies are required to clarify these relations to facilitate the future clinical application of this framework.

All the experiments of this study were conducted in anesthetized, open-chest dogs. Anesthesia and surgical trauma affect the cardiovascular system significantly (34). Whether this equilibrium framework can be applied to conscious, closed-chest animals (including humans) remains to be seen. We used two pumps for total heart bypass. However, it is well known that the CO of the two sides of the heart is not identical because of the anatomic shunt between the systemic and pulmonary circulations, e.g., the bronchial artery. However, the difference between the flow rates was <3% of CO. Therefore, it is unlikely that such a minor difference in CO would influence the conclusion of this study.

Conclusion

We were able to characterize the venous return properties of the systemic and pulmonary circulations in a simple manner using the flat venous return surface. Equating the standard venous return surface with the measured integrated CO curves, under a variety of stressed blood volumes and cardiac functions, enabled us to accurately predict hemodynamics.

APPENDIX

Concept of Integrated Venous Return

Using a distributed model, Sagawa and Sunagawa and their coworkers (24, 30) modeled the vascular system. Suppose that compliance and resistance are distributed in the systemic circulation (Fig. 10). When the compliance distribution [$C(x)$] and pressure distribution [$P(x)$] are expressed as a function of distance (x) from the venous port, then stressed blood volume (V_S) in the systemic circulation can be described as

$$V_s = \int_0^L P(x)C(x)dx \qquad (A1)$$

where L represents the distance between the arterial and venous ports. If we denote the cumulative resistance over a distance x from the venous port by $R(x)$, the serial pressure distribution can be expressed as

$$P(x) = R(x)CO_V + P_{RA} \qquad (A2)$$

Substituting *Eq. A2* into *Eq. A1* yields

$$V_S = CO_V \int_0^L C(x)R(x)dx + P_{RA} \int_0^L C(x)dx \qquad (A3)$$

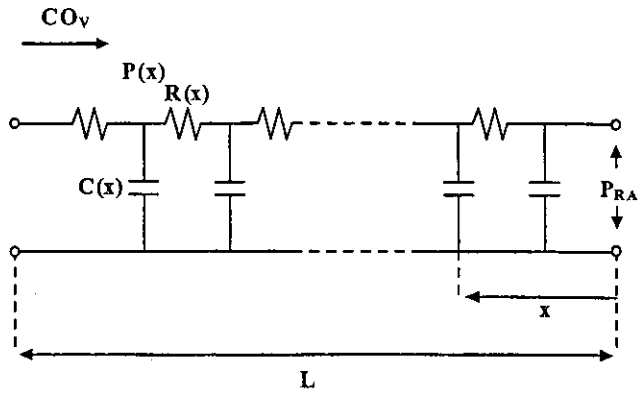

Fig. 10. Vascular system modeled by a distributed system. $C(x)$, $P(x)$, and $R(x)$, compliance, pressure, and cumulative resistance over a distance x from the venous port; L, distance between arterial and venous ports.

When $C_S D_{CS}(x)$ is substituted for $C(x)$, where C_S is the total systemic vascular compliance and $D_{CS}(x)$ is the normalized distribution of compliance as a function of x (thus $\int_0^L D_{CS}(x)dx$ is unity), *Eq. A3* can be rewritten as

$$V_S = CO_V C_S \int_0^L D_{CS}(x)R(x)dx + P_{RA}C_S \int_0^L D_{CS}(x)dx \qquad (A4)$$

The first integral term, which sums cumulative resistance weighted by systemic compliance distribution, is equivalent to the resistance for systemic venous return, R_{VS}, of Guyton et al. (16, 17). Because the second integral is unity, *Eq. A4* can be rewritten as

$$V_S = CO_V C_S R_{VS} + P_{RA}C_S \qquad (A5)$$

Stressed blood volume in the pulmonary circulation (V_P) can be related to CO_V and P_{LA} by the following equation

$$V_P = CO_V C_P R_{VP} + P_{LA}C_P \qquad (A6)$$

where C_P is the total pulmonary compliance and R_{VP} is the resistance for pulmonary venous return.

For a given condition, the sum of the stressed blood volumes in the systemic circulation and pulmonary circulation, V (i.e., $V_s + V_P$), remains constant, irrespective of its distribution. Thus adding *Eqs. A5* and *A6* and rearranging yields

$$CO_V = V/W - G_S P_{RA} - G_P P_{LA} \qquad (A7)$$

where W, G_S, and G_P are linear parameters and are expressed as

$$W = C_S R_{VS} + C_P R_{VP} \qquad (A8)$$

$$G_S = C_S/W \qquad (A9)$$

and

$$G_P = C_P/W \qquad (A10)$$

For a given V, CO_V can be related to P_{RA} and P_{LA} by a surface expressed by *Eq. A7* (Fig. 1*B*). When V is kept constant, CO_V decreases with increases in P_{RA} and/or P_{LA}.

From *Eqs. A8–A10*, once C_S, R_{VS}, C_P, and R_{VP} are given, we can estimate W, G_S, and G_P. Lee and Goldman (19) reported C_S as 1.9 $ml \cdot mmHg^{-1} \cdot kg^{-1}$ and R_{VS} as 0.056 $mmHg \cdot ml^{-1} \cdot min \cdot kg$ in eight dogs. Shoukas (26) reported C_P as 0.31 $ml \cdot mmHg^{-1} \cdot kg^{-1}$ and R_{VP} as 0.077 $mmHg \cdot ml^{-1} \cdot min \cdot kg$ in nine dogs. Estimated W, G_S, and G_P were 0.131 min, 14.56 $ml \cdot min^{-1} \cdot mmHg^{-1} \cdot kg^{-1}$, and 2.39 $ml \cdot min^{-1} \cdot mmHg^{-1} \cdot kg^{-1}$, respectively. These values are in good agreement with those obtained in our experiment.

ACKNOWLEDGMENTS

The authors gratefully acknowledge the technical assistance of Dr. Yoshiaki Takewa.

GRANTS

This study was supported by Japan Society for the Promotion of Science, Research, and Development Grant-In-Aid for Scientific Research C 14570707, a Ground-Based Research Grant for space utilization promoted by the National Space Development Agency of Japan and the Japan Space Forum, and the Program for Promotion of Fundamental Studies in Health Science of the Organization for Pharmaceutical Safety and Research of Japan.

REFERENCES

1. **Alexander RS.** Influence of constrictor drugs on the distensibility of the splanchnic venous system analyzed on the basis of an aortic model. *Circ Res* 2: 140–147, 1954.
2. **Braunwald E, Colucci WS, and Grossman W.** Clinical aspects of heart failure: high-output heart failure; pulmonary edema. In: *Heart Disease. A Textbook of Cardiovascular Medicine* (5th ed.), edited by Braunwald E. Philadelphia, PA: Saunders, 1997, p. 445–470.
3. **Brengelmann GL.** A critical analysis of the view that right atrial pressure determines venous return. *J Appl Physiol* 94: 849–859, 2003.
4. **Burkhoff D and Tyberg JV.** Why does pulmonary venous pressure rise after onset of LV dysfunction: a theoretical analysis. *Am J Physiol Heart Circ Physiol* 265: H1819–H1828, 1993.
5. **Caldini P, Permutt S, Waddell JA, and Riley RL.** Effect of epinephrine on pressure, flow, and volume relationships in the systemic circulation of dogs. *Circ Res* 34: 606–623, 1974.
6. **Chaliki HP, Hurrell DG, Nishimura RA, Reinke RA, and Appleton CP.** Pulmonary venous pressure: relationship to pulmonary artery, pulmonary wedge, and left atrial pressure in normal, lightly sedated dogs. *Catheter Cardiovasc Interv* 56: 432–438, 2002.
7. **Chen HI, Chang KC, and Hsieh KS.** Vascular factors in isovolumic systemic and pulmonary circuit. *Am J Physiol Heart Circ Physiol* 260: H201–H209, 1991.
8. **Den Hartog EA, Versprille A, and Jansen JR.** Systemic filling pressure in intact circulation determined on basis of aortic vs. central venous pressure relationships. *Am J Physiol Heart Circ Physiol* 267: H2255–H2258, 1994.
9. **Drees JA and Rothe CF.** Reflex venoconstriction and capacity vessel pressure-volume relationships in dogs. *Circ Res* 34: 360–73, 1974.
10. **Forrester JS, Diamond G, Chatterjee K, and Swan HJG.** Medical therapy of acute myocardial infarction by application of hemodynamic subsets. *N Engl J Med* 295: 1356–1362, 1976.
11. **Fuse K, Kodama M, Okura Y, Ito M, Hirono S, Kato K, Hanawa H, and Aizawa Y.** Predictors of disease course in patients with acute myocarditis. *Circulation* 102: 2829–2835, 2000.
12. **Glantz SA and Parmley WW.** Factors which affect the diastolic pressure-volume curve. *Circ Res* 42: 171–180, 1978.
13. **Grodins FS, Stuart WH, and Veenstra RL.** Performance characteristics of the right heart bypass preparation. *Am J Physiol* 198: 552–560, 1960.
14. **Guyton AC.** Determination of cardiac output by equating venous return curves with cardiac response curves. *Physiol Rev* 35: 123–129, 1955.
15. **Guyton AC, Jones CE, and Coleman TG.** *Circulatory Physiology: Cardiac Output and Its Regulation* (2nd ed.). Philadelphia, PA: Saunders, 1973, p. 237–252.
16. **Guyton AC, Lindsey AW, Abernathy B, and Richardson T.** Venous return at various right atrial pressures and the normal venous return curves. *Am J Physiol* 189: 609–615, 1957.
17. **Guyton AC, Lindsey AW, and Kaufmann BN.** Effect of mean circulatory filling pressure and other peripheral circulatory factors on cardiac output. *Am J Physiol* 180: 463–468, 1955.
18. **Harlan JC, Smith EE, and Richardson TQ.** Pressure-volume curves of systemic and pulmonary circuit. *Am J Physiol* 213: 1499–1503, 1967.
19. **Lee RW and Goldman S.** Mechanism for decrease in cardiac output with atrial natriuretic peptide in dogs. *Am J Physiol Heart Circ Physiol* 256: H760–H765, 1989.
20. **Levy MN.** The cardiac and vascular factors that determine systemic blood flow. *Circ Res* 44: 739–747, 1979.
21. **Lucas C, Johnson W, Hamilton MA, Fonarow GC, Woo MA, Flavell CM, Creaser JA, and Stevenson LW.** Freedom from congestion predicts good survival despite previous class IV symptoms of heart failure. *Am Heart J* 140: 840–847, 2000.
22. **Maughan WL, Sunagawa K, and Sagawa K.** Ventricular systolic interdependence: volume elastance model in isolated canine hearts. *Am J Physiol Heart Circ Physiol* 253: H1381–H1390, 1987.
23. **Ogilvie RI and Zborowska-Sluis D.** Effect of chronic rapid ventricular pacing on total vascular capacitance. *Circulation* 85: 1524–1530, 1992.
24. **Sagawa K, Maughan WL, Suga H, and Sunagawa K.** *Cardiac Contraction and Pressure-Volume Relationship.* Oxford, UK: Oxford Univ. Press, 1988, p. 232–298.
25. **Sarnoff SJ and Berglund E.** Ventricular function. 1. Starling's law of the heart, studied by means of simultaneous right and left ventricular function curves in the dog. *Circulation* 9: 706–718, 1953.
26. **Shoukas AA.** Pressure-flow and pressure-volume relations in the entire pulmonary vascular bed of the dog determined by two-port analysis. *Circ Res* 37: 809–818, 1975.

27. **Shoukas AA.** Carotid sinus baroreceptor reflex control and epinephrine. Influence on capacitive and resistive properties of the total pulmonary vascular bed of the dog. *Circ Res* 51: 95–101, 1982.
28. **Stone HL, Bishop VS, and Dong EJ.** Ventricular function in cardiac denervated and cardiac sympathectomized conscious dogs. *Circ Res* 20: 587–593, 1967.
29. **Sunagawa K, Maughan WL, Burkhoff D, and Sagawa K.** Left ventricular interaction with arterial load studied in isolated canine ventricle. *Am J Physiol Heart Circ Physiol* 245: H773–H780, 1983.
30. **Sunagawa K, Sagawa K, and Maughan WL.** Ventricular interaction with the loading system. *Ann Biomed Eng* 12: 163–189, 1984.
31. **Sylvester JT, Goldberg HS, and Permutt S.** The role of the vasculature in the regulation of cardiac output. *Clin Chest Med* 4: 111–126, 1983.
32. **Todaka K, Leibowitz D, Homma S, Fisher PE, Derosa C, Stennett R, Packer M, and Burkhoff D.** Characterizing ventricular mechanics and energetics following repeated coronary microembolization. *Am J Physiol Heart Circ Physiol* 272: H186–H194, 1997.
33. **Tyberg JV.** How changes in venous capacitance modulate cardiac output. *Pflügers Arch* 445: 10–17, 2002.
34. **Vatner SF and Braunwald E.** Cardiovascular control mechanisms in the conscious state. *N Engl J Med* 293: 970–976, 1975.
35. **Wang SY, Manyari DE, Scott-Douglas N, Smiseth OA, Smith ER, and Tyberg JV.** Splanchnic venous pressure-volume relation during experimental acute ischemic heart failure. Differential effects of hydralazine, enalaprilat, and nitroglycerin. *Circulation* 91: 1205–1212, 1995.

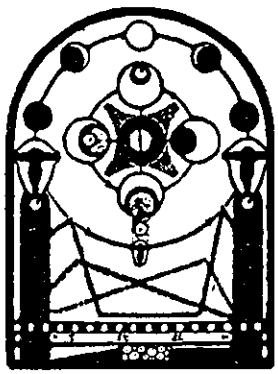

Reprinted from CIRCULATION, Volume 109, Number 1, January 6-13, 2004
Lippincott Williams & Wilkins Printed in U.S.A.

Vagal Nerve Stimulation Markedly Improves Long-Term Survival After Chronic Heart Failure in Rats

Meihua Li, MS; Can Zheng, PhD; Takayuki Sato, MD; Toru Kawada, MD;
Masaru Sugimachi, MD; Kenji Sunagawa, MD

Vagal Nerve Stimulation Markedly Improves Long-Term Survival After Chronic Heart Failure in Rats

Meihua Li, MS; Can Zheng, PhD; Takayuki Sato, MD; Toru Kawada, MD; Masaru Sugimachi, MD; Kenji Sunagawa, MD

Background—Diminished cardiac vagal activity and higher heart rate predict a high mortality rate of chronic heart failure (CHF) after myocardial infarction. We investigated the effects of chronic electrical stimulation of the vagus nerve on cardiac remodeling and long-term survival in an animal model of CHF after large myocardial infarction.

Methods and Results—Two weeks after the ligation of the left coronary artery, surviving rats were randomized to vagal- and sham-stimulated groups. Using an implantable miniature radio-controlled electrical stimulator, we stimulated the right vagal nerve of CHF rats for 6 weeks. The intensity of electrical stimulation was adjusted for each rat, so that the heart rate was lowered by 20 to 30 beats per minute. The treated rats had significantly lower left ventricular end-diastolic pressure (17.1±5.9 versus 23.5±4.2 mm Hg, $P<0.05$) and higher maximum dp/dt of left ventricular pressure (4152±237 versus 2987±192 mm Hg/s, $P<0.05$) than the untreated rats. Improvement of cardiac pumping function was accompanied by a decrease in normalized biventricular weight (2.75±0.25 versus 3.14±0.22 g/kg, $P<0.01$). Although the 140-day survival of the untreated group was only half, vagal stimulation markedly improved the survival rate (86% versus 50%, $P=0.008$). Vagal stimulation therapy achieved a 73% reduction in a relative risk ratio of death.

Conclusions—Vagal nerve stimulation markedly improved the long-term survival of CHF rats through the prevention of pumping failure and cardiac remodeling. (***Circulation.*** **2004;109:120-124.**)

Key Words: electrical stimulation ■ heart failure ■ myocardial infarction ■ remodeling ■ vagus nerve

Acute myocardial infarction[1] occurs when blood supply to part of the heart muscle is severely reduced or stopped. Survivors after large myocardial infarction have a high risk for chronic heart failure (CHF), with poor prognosis. CHF is a clinical syndrome that is initiated by cardiac dysfunction and followed by activation of compensatory mechanisms such as the sympathoadrenal and renin-angiotensin-aldosterone systems. Apparently, activation of compensatory mechanisms during the early phase of CHF helps the heart compensate for deteriorating pumping function. However, excessive sustained activation has deleterious effects on cardiac function. Once such an excessive activation, on the contrary, worsens cardiac function, it triggers further activation of those compensatory mechanisms, which, in turn, further deteriorates cardiac function. This positive feedback mechanism leads the heart to decompensatory cardiac remodeling and failure at the end stage. Therefore, the maladaptation process is a key of pathophysiology of CHF.

In the maladaptation process, the cardiac autonomic nervous system[2,3] also plays an important role. Clinical evidence from the Autonomic Tone and Reflexes After Myocardial Infarction study (ATRAMI)[4] and the Cardiac Insufficiency BIsoprolol Study II (CIBIS II)[5] indicates that diminished cardiac vagal activity and increased heart rate predict a high mortality rate of CHF. Based on this body of knowledge, it would be logical to clarify whether augmentation of vagal activity prevents cardiac remodeling and death. On the occurrence of life-threatening arrhythmias in acute ischemia, the effect of vagal stimulation has been reported to prevent ventricular fibrillation in dogs.[6] The antianginal effect of vagal stimulation has been also shown in patients with coronary artery disease.[7] However, its effect on CHF remains unknown. Therefore, in the present study, we examined the effects of vagal stimulation on cardiac remodeling after large myocardial infarction and on the long-term prognosis of CHF in rats.

Methods

Experimental Heart Failure

The care and use of the animals were in strict accordance with the guiding principles of the Physiological Society of Japan. Left ventricular myocardial infarction was induced by coronary artery ligation in 8-week-old male Sprague-Dawley rats (SLC, Hamamatsu, Japan). The mortality rate in animals with myocardial infarction was ≈60% within the first 24 hours. One week later, we checked the infarct size by echocardiography (SSA-380A, Toshiba), as described previously.[8] The rats with infarcted area >40% of the left ventricular

Received January 16, 2003; de novo received June 4, 2003; revision received August 25, 2003; accepted August 26, 2003.

From the Department of Cardiovascular Dynamics, National Cardiovascular Center Research Institute, Suita, Japan (M.L., C.Z., T.S., T.K., M.S., K.S.); and the Department of Cardiovascular Control, Kochi Medical School, Nankoku, Japan (T.S.).

Correspondence to Takayuki Sato, MD, Department of Cardiovascular Control, Kochi Medical School, Nankoku, Kochi 783-8505, Japan. E-mail tacsato-kochimed@umin.ac.jp

© 2004 American Heart Association, Inc.

Circulation is available at http://www.circulationaha.org

DOI: 10.1161/01.CIR.0000105721.71640.DA

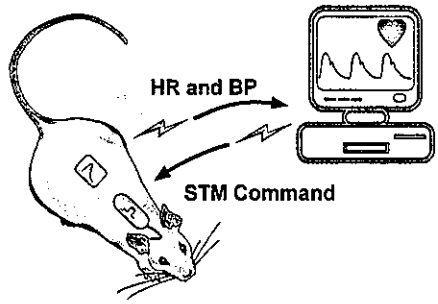

Figure 1. Neural interface approach to stimulate the vagal nerve. While monitoring heart rate through an implantable transmitter, a remote control system adjusted the intensity of electrical pulses of an implantable miniature radio-controlled electrical stimulator.

wall were enrolled in the present study. In sham-operated rats, we loosely tied a suture to avoid coronary artery occlusion. We confirmed the infarct size by postmortem examination.

Vagal Nerve Stimulation

To stimulate the vagal nerve and to monitor blood pressure and heart rate in freely moving rats, we developed a remote system controlled by a computer (Figure 1). The computer commands an implantable and radio-controlled pulse generator (ISE1010C, Unimec) to stimulate the vagal nerve while sensing blood pressure and heart rate through an implantable transmitter (TA11PA-C40, Data Sciences International). The miniature pulse generator and transmitter were subcutaneously implanted in the abdomen at 7 days after myocardial infarction. A pair of Teflon-coated stainless steel wires for electrical stimulation was looped around the right vagal nerve in the neck; a Teflon tube for blood pressure recording was placed in the abdominal aorta.

Experimental Protocols

At 14 days after myocardial infarction, the survivors were randomized into groups treated with sham and active stimulation. In the actively treated group, we stimulated the vagal nerve with electrical rectangular pulses of 0.2-ms duration at 20 Hz for 10 seconds every minute for 6 weeks. The electrical current of pulses was adjusted for each rat, so that the heart rate was lowered by 20 to 30 beats per minute. This resulted in the ranges of 0.1 to 0.13 mA. Mean blood pressure and heart rate were recorded every minute for 6 weeks. In a preliminary study, we confirmed that the chronic vagal stimulation at this intensity did not alter feeding behavior and did not evoke any signs of pain reaction such as an increase in plasma epinephrine level.

Hemodynamic and Remodeling Study

To evaluate the effect of vagal stimulation on cardiac remodeling, at the end of the 6-week stimulation period we measured hemodynamics and heart weights of sham-operated and sham-stimulated rats, untreated CHF rats, and treated CHF rats. Anesthesia was maintained through the use of 1.2% halothane during surgical procedures and 0.6% halothane during data recording. Left ventricular and arterial pressures were measured with a 2F catheter-tipped micromanometer (SPC-320, Millar Instruments). Pressure signals were digitized at a rate of 1 kHz for 5 minutes. After hemodynamic measurement, the heart was excised for subsequent determination of infarct size.

Prognosis and Neurohormone Study

To examine the effect of 6-week vagal stimulation on prognosis, we observed a 20-week survival rate in treated and untreated CHF rats. Because of the life of the battery of the implantable pulse generator, the treatment period was limited to 6 weeks. Each cage was inspected daily for the rat that had died. The heart was removed from the dead animal for subsequent determination of infarct size.

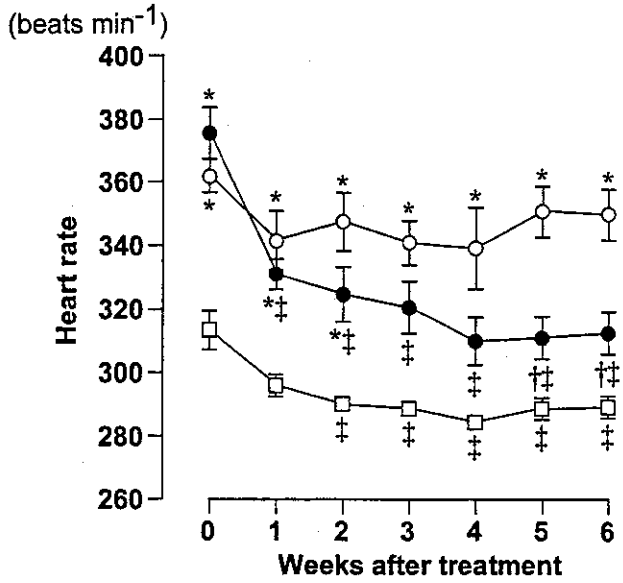

Figure 2. Effects of 6-week vagal nerve stimulation on 24-hour average of heart rate of sham-operated (SO-SS, □, n=9) rats treated with sham stimulation, CHF rats treated with sham (CHF-SS, ○, n=13), and vagal stimulation (CHF-VS, ●, n=11). Data are expressed as mean±SEM. *P<0.05 from SO-SS group; †P<0.05 from CHF-SS group; ‡P<0.05 from pretreatment values of each group.

At the end of the observation period, blood for neurohormone assays was sampled. The surviving rat was placed in a glass jar, where it inspired a mixture of 1.2% halothane in oxygen-enriched air for 5 to 10 minutes. To avoid the modification of neurohumoral states by invasive manipulation, immediately after the induction of anesthesia, we quickly collected 3 mL of a blood sample from the left ventricular cavity through a transthoracic approach without measuring hemodynamics. After blood sampling, the heart was excised for subsequent determination of infarct size.

Plasma concentrations of norepinephrine were measured by high-performance liquid chromatography with electrochemical detection. Plasma levels of brain natriuretic peptide were determined by radioimmunoassay.

Determination of Infarct Size

As described previously,[9] the right ventricle and the left ventricle including the interventricular septum were dissected, separated, and weighted. The heart was fixed in 10% buffered formalin. The left ventricle was cut from apex to base into 4 transverse slices. Sections 4 μm thick were cut and stained by Masson trichrome method. Histological images were digitized through a frame grabber and analyzed. Infarct size was calculated from the 4 slices by dividing the sum of the endocardial lengths of infarcted regions by the sum of the total endocardial circumferences.

Statistical Analysis

For data of the hemodynamic and remodeling study, differences among 3 groups were tested by ANOVA, with a Scheffé multiple comparison test. Differences in heart rates before and during treatment in each group were examined by a 1-way ANOVA with repeated measures, followed by a post hoc Dunnett test.

For a neurohormonal data, differences between two groups were examined by a Mann-Whitney U test. Survival data are presented as Kaplan-Meier curves; the effect of treatment on 140-day survival was analyzed by a Fisher exact test. Differences were considered significant at a value of P<0.05.

Mean Blood Pressure (mm Hg)

		Weeks After Stimulation					
Group	Before	1	2	3	4	5	6
SO-SS	104±2	104±3	104±3	103±3	102±3	102±2	104±3
CHF-SS	83±3*	83±6*	83±6*	83±9*	85±9*	83±7*	81±6*
CHF-VS	85±10*	82±5*	82±7*	81±7*	80±7*	82±6*	83±7*

SO-SS indicates sham-operated rats treated with sham stimulation (SS); CHF-SS, CHF rats treated with sham stimulation; CHF-VS, CHF rats treated with vagal stimulation. Values are mean±SD of the 24-hour average of mean blood pressure.

*$P<0.01$ from SO-SS group.

Results

Hemodynamic and Remodeling Study

Although CHF rats (untreated, n=13; treated, n=11) had a higher heart rate than sham-operated rats (n=9) before the treatment, vagal stimulation significantly slowed the heart rate of CHF rats (Figure 2). The difference in heart rate between untreated and treated CHF rats reached ≈40 beats per minute at the end of treatment ($P<0.05$). CHF rats had significantly lower blood pressure, but the vagal stimulation did not affect blood pressure during the 6-week treatment period (Table).

When compared with sham-operated rats, untreated CHF rats had low blood pressure (Figure 3a), high left ventricular end-diastolic pressure (LVEDP) (Figure 3b), a depressed maximum dp/dt of left ventricular pressure ($LV+dp/dt_{max}$) (Figure 3c), and an increased heart weight (Figure 3d). On the other hand, CHF rats treated with vagal nerve stimulation had significantly lower LVEDP (17.1±5.9 versus 23.5±4.2 mm Hg, $P<0.05$) and higher $LV+dp/dt_{max}$ (4152±237 versus 2987±192 mm Hg/s, $P<0.05$) than untreated CHF rats. Improvement of pumping function in treated CHF rats was accompanied by a significant decrease in normalized biventricular weight (2.75±0.25 versus 3.14±0.22 g/kg, $P<0.01$). There was no significant difference in infarct size between treated and untreated CHF rats (53±7% versus 53±6%).

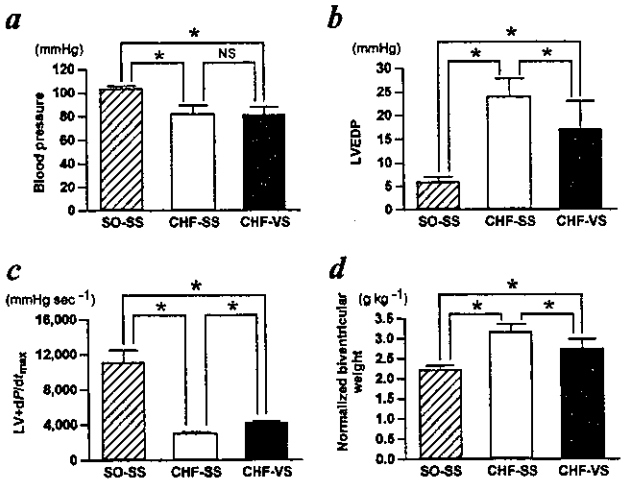

Figure 3. Effects of vagal nerve stimulation on a, mean blood pressure; b, LVEDP; c, maximum dp/dt of left ventricular pressure ($LV+dP/dt_{max}$); d, biventricular weight normalized by body weight in sham-operated (SO-SS, hatched bar, n=9) rats treated with sham stimulation, CHF rats treated with sham (CHF-SS, open bar, n=13), and vagal stimulation (CHF-VS, closed bar, n=11). Assessment was made at the end of 6-week treatment. Data are expressed as mean±SD. *$P<0.05$; ‡$P<0.01$.

Prognosis and Neurohormone Study

Although 60 rats with CHF after large myocardial infarction were enrolled in the prognosis study, 8 of the 30 rats assigned to the treated group were excluded from the results because of the breaking down of electrode wires during vagal stimulation for 6 weeks. Vagal nerve stimulation markedly suppressed the mortality rate of CHF rats (Figure 4); there were only 3 deaths among the 22 treated rats versus 15 deaths among the 30 untreated rats (14% versus 50%, $P=0.008$). Vagal stimulation therapy achieved a 73% reduction in a relative risk ratio of death.

Shown in Figure 5, improvement of survival in treated CHF rats was accompanied by a significant decrease in normalized biventricular weight (2.63±0.38 versus 3.17±0.42 g/kg, $P<0.01$). When compared with untreated CHF rats, treated CHF rats had lower levels of plasma norepinephrine (426±102 versus 1182±260 pg/mL, $P<0.01$) and brain natriuretic peptide (251±31 versus 363±82 pg/mL, $P<0.01$). There was no significant difference in infarct size between treated and untreated CHF rats (54±8% versus 53±7%).

Discussion

The prognosis of patients with CHF is still poor, even though various therapeutic approaches with a β-adrenergic receptor

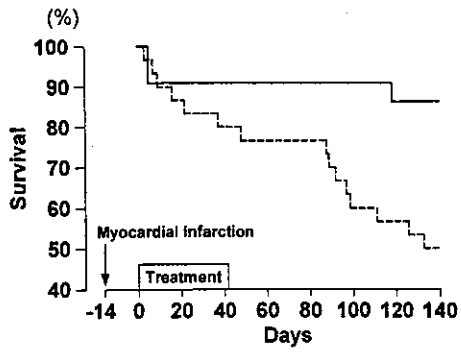

Figure 4. Effects of vagal nerve stimulation on survival curves of CHF rats treated with sham (broken line, n=30) and vagal stimulation (solid line, n=22). Treatment started 14 days after coronary artery ligation. Vagal stimulation significantly ($P=0.008$) improved survival rate.

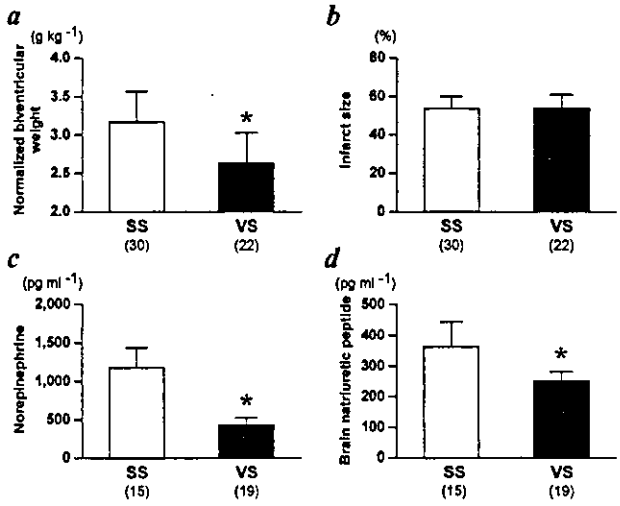

Figure 5. Comparison of biventricular weight normalized by body weight (a), infarct size (b), and plasma levels of norepinephrine (c) and brain natriuretic peptide (d) in CHF rats treated with sham stimulation (SS) and vagal stimulation (VS). Each value in parentheses indicates number of animals in each group. *$P<0.01$.

blocker,[10,11] angiotensin-converting enzyme inhibitor,[12] angiotensin-receptor blocker,[13] aldosterone antagonist,[14] and implantable defibrillator[15] are currently available. Therefore, more effective modality of therapy is expected.

The present results indicate that vagal nerve stimulation markedly improved the long-term survival of CHF rats through prevention of the progression of pumping failure and cardiac remodeling. The main objective of the present study was to test the working hypothesis that long-term vagal stimulation can improve survival of CHF rats after large myocardial infarction, not to clarify the mechanism. However, some considerations on this issue are warranted.

It is conceivable that vagal stimulation may effectively sever the vicious cycle leading to death through an inhibitory effect on presynaptic norepinephrine releases and suppressive effects on adrenergic signaling cascade through G-protein interactions.[16] In human hearts as well as those of several other species, muscarinic receptors are predominantly of the M_2-subtype, which couples through a pertussis toxin–sensitive G_i protein to inhibit adenyl cyclase. In the atrium, stimulation of muscarinic M_2 receptors causes direct negative inotropic and chronotropic effects; in the ventricle, on the other hand, the negative inotropic effect can be only achieved when the basal level of cAMP is elevated by β-adrenoceptor agonists. These mechanisms are known as accentuated antagonism.

Vagal stimulation is also postulated to improve ventricular efficiency by slowing heart rate.[17] Burkhoff et al[18] showed that the ventricular efficiency, that is, the ratio of ventricular stroke work to ventricular oxygen consumption, is adjusted to be maximal under physiological conditions and that the efficiency of the failing heart is more sensitive to changes in heart rate than that of the normal heart. Prevention of tachycardia after myocardial infarction by vagal stimulation would optimize the efficiency of the failing heart and thus protect the heart against remodeling.

Apparently, vagal efferent stimulation is considered to act on the ventricle of CHF like a β-adrenergic blocker. However, in rats, β-blockade therapy rather failed to exert a beneficial effect on the cardiac remodeling or hemodynamics after myocardial infarction (for review, see Gaballa and Goldman[19]). Litwin et al[20] showed that chronic propranolol treatment did not improve cardiac remodeling and worsened pumping function in rats with postinfarction CHF. Wei et al[21] also demonstrated that metoprolol deteriorated ventricular remodeling in CHF rats. Therefore, in addition to antagonism against sympathetic effects, unique actions of vagal stimulation would be important in providing the favorable outcome for CHF rats. A facilitatory effect of vagal stimulation on nitric oxide release from the coronary endothelium could also have an antiremodeling action through improvement of viable myocardial conditions.[22]

In addition to the effects of electrical stimulation of vagal efferents on the heart, vagal afferent effects[7,23] are also considered because afferent stimulation would evoke cardiopulmonary reflex and modulate neuronal activity in several hypothalamic nuclei involved in cardiovascular regulation. As shown in Figure 5c, vagal stimulation lowered the plasma norepinephrine level. Therefore, vagal stimulation therapy would terminate the vicious circle of maladaptation in CHF through the suppression of chronic excessive activation of the sympathetic nervous system.[24,25]

A more recent study by Guarini et al[26] has shown that efferent vagal fiber stimulation blunts activation of nuclear factor-κB in the liver through nicotinic receptors and then reduces the hepatic production and the plasma level of tumor necrosis factor-α during acute hemorrhagic shock. It has been reported that these factors are also involved in cardiac remodeling and the poor prognosis of CHF.[27] Therefore, the hepatic effect of vagal stimulation would prevent cardiac remodeling and improve survival of CHF.

It is also noted that short-term vagal stimulation for 6 weeks after myocardial infarction prevented long-term cardiac remodeling (Figure 5a) and improved the long-term survival. There may be a critical period during which short-term treatment against cardiac dysfunction and remodeling will ensure the long-term survival of CHF.

A pioneer work by Pfeffer et al[28] examined the effect of long-term therapy with captopril in CHF rats after myocardial infarction. As well as vagal stimulation in the present study, oral captopril administration started at 14 days after ligation of the left coronary artery. Pfeffer et al observed 1-year survival and found that the median survival was 146 and 181 days for untreated and treated CHF rats with large infarcts, respectively. Thus, the survival curve of untreated CHF rats with large infarcts in their study was quite similar to our result of untreated CHF rats. On the other hand, the effect of captopril on survival in CHF rats with large infarcts appeared to be much different from that of vagal stimulation. Approximately 40% of captopril-treated CHF rats with large infarcts died at 140 days; vagal stimulation reduced the mortality rate to <20%. Therefore, vagal stimulation therapy may be promising for severe CHF after large myocardial infarction.

Limitations

The beneficial effects of vagal stimulation on cardiac function, remodeling, and survival of CHF rats were shown in the present study. However, its safety and adverse effects remain to be unclear. The appropriate protocol of treatment is also still unsettled and should be investigated. To establish the therapeutic strategy shown in this study, large-scale, long-term trials of vagal nerve stimulation with an animal model of CHF are required.

Clinical Implications

Our previous studies[9,29] indicated that a pharmacological intervention in the central nervous system of CHF rats prevented the progression of cardiac dysfunction and remodeling. The therapeutic modality used in the present study also brought a favorable prognosis of CHF by manipulation of autonomic tone through vagal efferent and/or afferent mechanisms. We therefore propose the neural interface approach to optimize cardiac autonomic tone for the treatment of CHF. Technologies to materialize this neural interface strategy[30] using totally implantable miniaturized systems are readily available.[31,32]

Acknowledgments

This study was supported by a Health and Labor Sciences Research Grant (H14-NANO-002) for Advanced Medical Technology from the Ministry of Health, Labor, and Welfare of Japan, a Ground-Based Research Grant for the Space Utilization from NASDA and Japan Space Forum, and a Research Grant from Mitsubishi Pharma Research Foundation.

References

1. Pfeffer MA. Left ventricular remodeling after acute myocardial infarction. *Annu Rev Med.* 1995;46:455–466.
2. Cerati D, Schwartz PJ. Single cardiac vagal fiber activity, acute myocardial ischemia, and risk for sudden death. *Circ Res.* 1991;69:1389–1401.
3. Schwartz PJ, La Rovere MT, Vanoli E. Autonomic nervous system and sudden cardiac death: experimental basis and clinical observations for post-myocardial infarction risk stratification. *Circulation.* 1992;85(suppl I):I-77–I-91.
4. La Rovere MT, Bigger JT Jr, Marcus FI, et al. Baroreflex sensitivity and heart-rate variability in prediction of total cardiac mortality after myocardial infarction. *Lancet.* 1998;351:478–484.
5. Lechat P, Hulot JS, Escolano S, et al. Heart rate and cardiac rhythm relationships with bisoprolol benefit in chronic heart failure in CIBIS II trial. *Circulation.* 2001;103:1428–1433.
6. Vanoli E, De Ferrari GM, Stramba-Badiale M, et al. Vagal stimulation and prevention of sudden death in conscious dogs with a healed myocardial infarction. *Circ Res.* 1991;68:1471–1481.
7. Zamotrinsky A, Kondratiev, de Jong JW. Vagal neurostimulation in patients with coronary artery disease. *Auton Neurosci Basic Clin.* 2001;88:109–116.
8. Litwin SE, Katz SE, Morgan JP, et al. Serial echocardiographic assessment of left ventricular geometry and function after large myocardial infarction in the rat. *Circulation.* 1994;89:345–354.
9. Sato T, Yoshimura R, Kawada T, et al. The brain is a possible target for an angiotensin-converting enzyme inhibitor in the treatment of chronic heart failure. *J Card Fail.* 1998;4:139–144.
10. Nagatsu M, Spinale FG, Koide M, et al. Bradycardia and the role of β-blockade in the amelioration of left ventricular dysfunction. *Circulation.* 2000;101:653–659.
11. Packer M, Coats AJ, Fowler MB, et al. Effect of carvedilol on survival in severe heart failure. *N Engl J Med.* 2001;344:1651–1658.
12. Yusuf S, Sleight P, Pogue J, et al. Effects of an angiotensin-converting-enzyme inhibitor, ramipril, on cardiovascular events in high-risk patients. *N Engl J Med.* 2000;342:145–153.
13. Cohn JN, Tognoni GA. Randomized trial of the angiotensin-receptor blocker valsartan in chronic heart failure. *N Engl J Med.* 2001;345:1667–1675.
14. Pitt B, Zannad F, Remme WJ, et al. The effect of spironolactone on morbidity and mortality in patients with severe heart failure. *N Engl J Med.* 1999;341:709–717.
15. Moss AJ, Zareba W, Hall WJ, et al. Prophylactic implantation of a defibrillator in patients with myocardial infarction and reduced ejection fraction. *N Engl J Med.* 2002;346:877–883.
16. Giessler C, Dhein S, Ponicke K, et al. Muscarinic receptors in the failing human heart. *Eur J Pharmacol.* 1999;375:197–202.
17. Schoemaker RG, Saxena PR, Kalkman EAJ. Low-dose aspirin improves in vivo hemodynamics in conscious, chronically infarcted rats. *Cardiovasc Res.* 1998;37:108–114.
18. Burkhoff D, Sagawa K. Ventricular efficiency predicted by an analytic model. *Am J Physiol.* 1986;250:R1021–R1027.
19. Gaballa MA, Goldman S. Ventricular remodeling in heart failure. *J Card Fail.* 2002;8:S476–S485.
20. Litwin SE, Katz SE, Morgan JP, et al. Effects of propranolol treatment on left ventricular function and intracellular calcium regulation in rats with postinfarction heart failure. *Br J Pharmacol.* 1999;127:1671–1679.
21. Wei S, Chow LTC, Sanderson JE. Effect of carvedilol in comparison with metoprolol on myocardial collagen postinfarction. *J Am Coll Cardiol.* 2000;36:276–281.
22. Zhao G, Shen W, Xu X, et al. Selective impairment of vagally mediated, nitric oxide-dependent coronary vasodilation in conscious dogs after pacing-induced heart failure. *Circulation.* 1995;91:2655–2663.
23. Mark AL. Sensitization of cardiac vagal afferent reflexes at the sensory receptor level: an overview. *Fed Proc.* 1987;46:36–40.
24. Swedberg K, Eneroth P, Kjekshus J, et al. Hormones regulating cardiovascular function in patients with severe congestive heart failure and their relation to mortality. *Circulation.* 1990;82:1730–1736.
25. Ceiler DL, Schiffers PMH, Nelissen-Vrancken HJMG, et al. Time-related adaptation in plasma neurohormone levels and hemodynamics after myocardial infarction in the rat. *J Card Fail.* 1998;4:131–138.
26. Guarini S, Altavilla D, Cainazzo, MM, at al. Efferent vagal fiber stimulation blunts nuclear factor-κB activation and protects against hypovolemic hemorrhagic shock. *Circulation.* 2003;107:1189–1194.
27. Mann DL. Tumor necrosis factor-induced signal transduction and left ventricular remodeling. *J Card Fail.* 2002;8:S379–S386.
28. Pfeffer MA, Pfeffer JM, Steinberg C, et al. Survival after an experimental myocardial infarction: beneficial effects of long-term therapy with captopril. *Circulation.* 1985;72:406–412.
29. Yoshimura R, Sato T, Kawada T, et al. Increased brain angiotensin receptor in rats with chronic high-output heart failure. *J Card Fail.* 2000;6:66–72.
30. Sato T, Kawada T, Sugimachi M, et al. Bionic technology revitalizes native baroreflex function in rats with baroreflex failure. *Circulation.* 2002;106:730–734.
31. Reid SA. Surgical technique for implantation of the neurocybernetic prosthesis. *Epilepsia.* 1990;31(suppl 2):S38–S39.
32. Murphy JV, Patil A. Stimulation of the nervous system for the management of seizures: current and future developments. *CNS Drugs.* 2003;17:101–115.

Am J Physiol Heart Circ Physiol 286: H1382–H1388, 2004.
First published November 20, 2003; 10.1152/ajpheart.00801.2003.

Muscle mechanoreflex induces the pressor response by resetting the arterial baroreflex neural arc

Kenta Yamamoto,[1] Toru Kawada,[1] Atsunori Kamiya,[1] Hiroshi Takaki,[1] Tadayoshi Miyamoto,[1,2] Masaru Sugimachi,[1] and Kenji Sunagawa[1]

[1]*Department of Cardiovascular Dynamics, National Cardiovascular Center Research Institute, Osaka 565-8565; and* [2]*Japan Association for the Advancement of Medical Equipment, Tokyo 113-0033, Japan*

Submitted 29 August 2003; accepted in final form 19 November 2003

Yamamoto, Kenta, Toru Kawada, Atsunori Kamiya, Hiroshi Takaki, Tadayoshi Miyamoto, Masaru Sugimachi, and Kenji Sunagawa. Muscle mechanoreflex induces the pressor response by resetting the arterial baroreflex neural arc. *Am J Physiol Heart Circ Physiol* 286: H1382–H1388, 2004. First published November 20, 2003; 10.1152/ajpheart.00801.2003.—The effects of the muscle mechanoreflex on the arterial baroreflex neural control have not previously been analyzed over the entire operating range of the arterial baroreflex. In anesthetized, vagotomized, and aortic-denervated rabbits (n = 8), we isolated carotid sinuses and changed intracarotid sinus pressure (CSP) from 40 to 160 mmHg in increments of 20 mmHg every minute while recording renal sympathetic nerve activity (SNA) and arterial pressure (AP). Muscle mechanoreflex was induced by passive muscle stretch (5 kg of tension) of the hindlimb. Muscle stretch shifted the CSP-SNA relationship (neural arc) to a higher SNA, whereas it did not affect the SNA-AP relationship (peripheral arc). SNA was almost doubled [from 63 ± 15 to 118 ± 14 arbitrary units (au), $P < 0.05$] at the CSP level of 93 ± 8 mmHg, and AP was increased ~50% by muscle stretch. When the baroreflex negative feedback loop was closed, muscle stretch increased SNA from 63 ± 15 to 81 ± 21 au ($P < 0.05$) and AP from 93 ± 8 to 109 ± 12 mmHg ($P < 0.05$). In conclusion, the muscle mechanoreflex resets the neural arc to a higher SNA, which moves the operating point towards a higher SNA and AP under baroreflex closed-loop conditions. Analysis of the baroreflex equilibrium diagram indicated that changes in the neural arc induced by the muscle mechanoreflex might compensate for pressure falls resulting from exercise-induced vasodilatation.

sympathetic nerve activity; arterial pressure; baroreflex equilibrium diagram; exercise pressor reflex; exercise

THE ARTERIAL BAROREFLEX plays an important role in stabilization of arterial pressure (AP) during daily activity. The input-output relationship of the arterial baroreflex system between baroreceptor pressure input and the resultant AP approximates a sigmoidal stimulus-response curve (19). This stimulus-response curve is known to reset toward a higher AP during exercise (7, 8, 23, 24, 29, 30, 34, 35). Recently, it was reported that exercise shifted the baroreflex curve for sympathetic nerve activity (SNA) to a higher SNA (5, 26). However, the neural mechanism responsible for the changes in baroreflex during exercise remains unclear. During exercise, AP and SNA are regulated by central command and the exercise pressor reflex (15, 22, 27, 42). The exercise pressor reflex is evoked by afferent inputs from metabolic (muscle metaboreflex)- and mechanical (muscle mechanoreflex)-sensitive skeletal muscle receptors. The muscle mechanoreflex has a dominant role in the exercise pressor reflex (6, 9, 20). We therefore hypothesized that the muscle mechanoreflex would reset the carotid sinus baroreflex control of SNA toward a higher SNA, evoking a pressor response under baroreflex closed-loop conditions. Earlier studies have reported that the muscle mechanoreflex reset the arterial baroreflex for AP and/or heart rate (13, 32). In the present study, we aimed to quantitatively investigate the effect of the muscle mechanoreflex on the carotid sinus baroreflex control of SNA.

Although the neural mechanism involved in resetting the baroreflex may be best analyzed using the baroreflex equilibrium diagram (28, 38), to the best of our knowledge, the effects of the muscle mechanoreflex on baroreflex function have never been assessed using this method. The baroreflex equilibrium diagram consists of the neural and peripheral arcs. The neural arc represents the static input-output relationship between baroreceptor pressure input and SNA, and the peripheral arc represents the relationship between SNA and AP. The intersection of the neural and peripheral arcs defines the operating point of the AP regulation under baroreflex closed-loop conditions (see *Theoretical considerations: coupling of neural and peripheral arcs* in MATERIALS AND METHODS for details).

To construct the baroreflex equilibrium diagram, we performed an open-loop experiment on the carotid sinus baroreflex in anesthetized rabbits (16–18, 38). The muscle mechanoreflex was induced by passive muscle stretch of the triceps surae muscle. The results of the present study indicate that the muscle mechanoreflex resets the baroreflex neural arc to a higher SNA, moving the operating point toward a higher AP under baroreflex closed-loop conditions.

MATERIALS AND METHODS

Theoretical considerations: coupling of neural and peripheral arcs. Changes in AP are immediately sensed by arterial baroreceptors, which alter efferent SNA via the arterial baroreflex. Efferent SNA, in turn, governs heart rate and the mechanical properties of the heart and vessels, which themselves exert a direct influence over AP. This cyclical negative feedback makes it difficult to analyze the behavior of the arterial baroreflex. To overcome this problem, we opened the negative feedback loop and divided the system into controlling and controlled elements (28). We defined the controlling element as a neural arc and the controlled element as a peripheral arc. In the neural arc, the input is the pressure sensed by the arterial baroreceptors and the output is SNA. In the peripheral arc, the input is SNA and the output is AP. Because pressure sensed by the arterial baroreceptor is

Address for reprint requests and other correspondence: K. Yamamoto, Dept. of Cardiovascular Dynamics, National Cardiovascular Center Research Institute, 5-7-1 Fujishirodai, Suita, Osaka 565-8565, Japan (E-mail: kentay@ri.ncvc.go.jp).

The costs of publication of this article were defrayed in part by the payment of page charges. The article must therefore be hereby marked "*advertisement*" in accordance with 18 U.S.C. Section 1734 solely to indicate this fact.

0363-6135/04 $5.00 Copyright © 2004 the American Physiological Society

equilibrated with AP under physiological conditions, we superimposed the functions of the two arcs and determined the operating point of the system from the intersection of the two arcs. The operating point is defined as the AP and SNA under closed-loop conditions of the feedback system. The validity of this framework has been examined in a previous study (38). Using the baroreflex equilibrium diagram, we aimed to quantify the effects of the muscle mechanoreflex on the carotid sinus baroreflex.

Surgical preparations. Animals were cared for in strict accordance with the Guiding Principles for the Care and Use of Animals in the Field of Physiological Sciences approved by the Physiological Society of Japan. Japanese White rabbits weighing 2.3–3.1 kg were anesthetized via an intravenous injection (2 ml/kg) with a mixture of urethane (250 mg/ml) and α-chloralose (40 mg/ml) and mechanically ventilated with oxygen-enriched room air. Arterial blood was sampled from the left common carotid artery. The rabbits were slightly hyperventilated to suppress chemoreflexes (arterial Pco_2 ranged from 30 to 35 mmHg, arterial $Po_2 > 300$ mmHg). Arterial blood pH was within the physiological range when rabbits were examined at the end of the surgical preparation and also at the end of the experiment. Supplemental anesthetics were administered continuously to maintain an appropriate level of anesthesia (0.3 $ml \cdot kg^{-1} \cdot h^{-1}$). The body temperature of each animal was maintained at ~38°C with a heating pad. AP was measured using a high-fidelity pressure transducer (Millar Instruments; Houston, TX) inserted retrogradely from the right common carotid artery to the aortic arch.

We isolated the bilateral carotid sinuses from the systemic circulation by ligating the internal and external carotid arteries and other small branches originating from the carotid sinus region. The isolated carotid sinuses were filled with warmed physiological saline via catheters inserted through the common carotid arteries. Intracarotid sinus pressure (CSP) was controlled by a servo-controlled piston pump (model ET-126A, Labworks; Costa Mesa, CA). Bilateral vagal and aortic depressor nerves were sectioned at the neck to eliminate baroreflexes from the cardiopulmonary region and aortic arch.

We exposed the left renal sympathetic nerve retroperitoneally and attached a pair of stainless steel wire electrodes (Bioflex wire AS633, Cooner Wire) to record SNA. The nerve bundle peripheral to the electrodes was tightly ligated and crushed to eliminate afferent signals from the kidney. The nerve and electrodes were secured with silicone glue (Kwik-Sil, World Precision Instruments; Sarasota, FL). The preamplified nerve signal was band-pass filtered at 150–1,000 Hz. It was then full-wave rectified and low-pass filtered with a cutoff frequency of 30 Hz to quantify the nerve activity. Pancuronium bromide (0.1 mg/kg) was administered to prevent contamination of SNA recordings by muscular activity.

With the rabbit in the prone position, the sacrum and the left ankle were clamped with a custom-made apparatus to prevent body trunk and hindlimb movement during muscle stretch. The left triceps surae muscle, Achilles tendon, and calcaneus bone were exposed. The left triceps surae muscle was isolated from surrounding tissue. The Achilles tendon was severed from the calcaneus bone and attached to a force transducer (Load Cell LUR-A-SA1, Kyowa Electronic Instruments; Tokyo, Japan). During muscle stretch, the force transducer was also connected to a 5-kg weight via a pulley, which opposed the Achilles tendon.

Protocols. Fourteen rabbits were used in the present study. Two rabbits were subjected to both *protocols 1* and *2* as described below.

In *protocol 1*, we examined the time course of the SNA response to stepwise muscle stretch ($n = 8$). Before muscle stretch, CSP was adjusted to instantaneous AP, and the operating point was determined from mean AP at steady state. CSP was then fixed at the operating point, and the left triceps surae muscle was stretched at 5 kg for 7 min.

In *protocol 2a*, we obtained the baroreflex equilibrium diagram under both control and muscle stretch conditions ($n = 8$). CSP was first decreased to 40 mmHg. After attainment of a steady state, CSP was then increased from 40 to 160 mmHg in increments of 20 mmHg. Each pressure step was maintained for 60 s. When SNA was completely suppressed and AP had fallen below 50 mmHg at the CSP level of 140 mmHg, the CSP level of 160 mmHg was omitted to prevent deterioration of the animal's condition. Thus the maximum duration of muscle stretch was 7 min. The order of control and muscle stretch conditions was randomized across the animals. In five of eight animals, the estimation of the baroreflex equilibrium diagram was repeated under both control and muscle stretch conditions after the left tibial nerve was severed.

In *protocol 2b*, we measured the actual operating point in the same eight animals that were used in *protocol 2a* to determine the accuracy of the operating point derived from the baroreflex equilibrium diagram. The operating point of the carotid sinus baroreflex was defined as the point where CSP equals AP (38). To obtain the actual operating point, CSP was adjusted to match AP via the servo-controlled system so that the carotid sinus baroreflex was virtually closed. After a steady state was reached, mean AP (and thus CSP) and SNA were taken as the values defining the actual operating point under control conditions. We also performed muscle stretch for 1 min while the carotid sinus baroreflex was virtually closed and obtained mean AP and SNA values defining the actual operating point during the last 10 s of muscle stretch.

Data analysis. We recorded CSP, SNA, and AP at a sampling rate of 200 Hz using a 12-bit analog-to-digital converter. Data were stored on the hard drive of a dedicated laboratory computer system for later analyses.

In *protocol 2a*, we calculated mean SNA and AP during the last 10 s of each CSP step. Because the absolute magnitude of SNA depended on recording conditions, SNA was presented in arbitrary units (au) so that the minimum and maximum values of SNA data obtained under control conditions were set to zero and 100 au, respectively, for each animal. A four-parameter logistic function analysis was performed on the neural arc (CSP-SNA data pairs) and the peripheral arc (SNA-AP data pairs) as follows (19)

$$y = \frac{P_1}{1 + \exp[P_2(x - P_3)]} + P_4 \qquad (1)$$

where x and y represent the input and the output, respectively; P_1 denotes the response range (i.e., the difference between the maximum and minimum values of y); P_2 is the coefficient of gain; P_3 defines the midpoint of the logistic function on the input axis; and P_4 represents the minimum value of y. The maximum gain (G_{max}) is $-P_1P_2/4$ at $x = P_3$.

In *protocol 2b*, we measured the actual operating point by closing the arterial baroreflex negative feedback loop. Mean SNA and AP values were obtained by averaging 10-s data at the steady state under both control and muscle stretch conditions.

Statistical analysis. All data are presented as means ± SD. Differences were considered significant when $P < 0.05$. The effects of muscle stretch on the parameters of the neural and peripheral arcs and operating points were examined using the paired t-test. The operating point as determined from the equilibrium diagram (*protocol 2a*) was compared with the operating point actually measured (*protocol 2b*) using linear regression analysis.

RESULTS

Figure 1 shows the group-averaged step response of SNA to muscle stretch. These data were collected under baroreflex open-loop conditions where CSP was fixed at an operating point of each animal. CSP was 87 ± 14 mmHg across all the animals. Muscle stretch transiently decreased and then increased SNA. The SNA value at 7 min was maintained at 93 ± 9% of the SNA at 1 min.

Figure 2 shows a typical time series of CSP, SNA, and AP under control conditions (*left*) and muscle stretch conditions

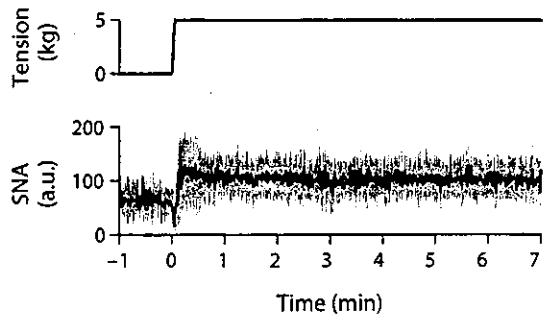

Fig. 1. Step response of sympathetic nerve activity [SNA; in arbitrary units (au)] to muscle stretch obtained from *protocol 1*. SNA transiently decreased and then increased during muscle stretch. The SNA response reached a steady state within ~40 s. The SNA value at 7 min was maintained at 93 ± 9% of the value observed at 1 min. The solid line indicates the mean value and the gray area represents means ± SD. Data were resampled at 1 Hz.

(*right*) obtained from *protocol 2a*. SNA and AP decreased in response to the increments in CSP under both control and muscle stretch conditions. Muscle stretch increased SNA and AP at CSP levels up to 100 mmHg in this animal.

Figure 3 illustrates the baroreflex neural arcs (*A*) and peripheral arcs (*B*) derived from the same data employed in Fig. 2. The open and closed circles represent data points obtained under control and muscle stretch conditions, respectively. The thin and thick solid lines indicate the fitted logistic functions under control and muscle stretch conditions, respectively. In the neural arcs, SNA decreased in response to the increments in CSP under both conditions. Muscle stretch increased SNA at CSP levels up to 100 mmHg. In the peripheral arcs, AP positively correlated with SNA. Peripheral arcs obtained under both conditions were nearly identical.

Figure 3*C* depicts the baroreflex equilibrium diagrams combined from Fig. 3, *A* and *B*. The thin and thick solid lines indicate the fitted logistic functions under control and muscle stretch conditions, respectively. Because CSP is equilibrated with AP under physiological conditions, the operating point is determined from the intersection of the neural and peripheral arcs. Muscle stretch moved the operating point toward higher SNA and AP (from *point a* to *point b*).

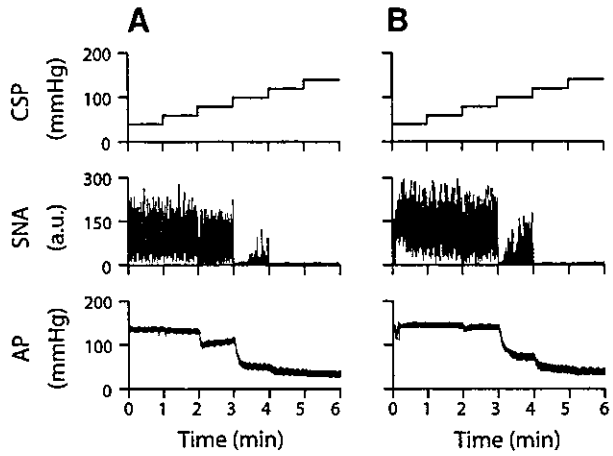

Fig. 2. Typical time series of intracarotid sinus pressure (CSP), SNA, and arterial pressure (AP) under control conditions (*A*) and muscle stretch conditions (*B*) obtained from *protocol 2a*. Data were resampled at 10 Hz. SNA and AP decreased in response to increments in CSP under both control and muscle stretch conditions. Muscle stretch increased SNA and AP at CSP levels up to 100 mmHg in this animal.

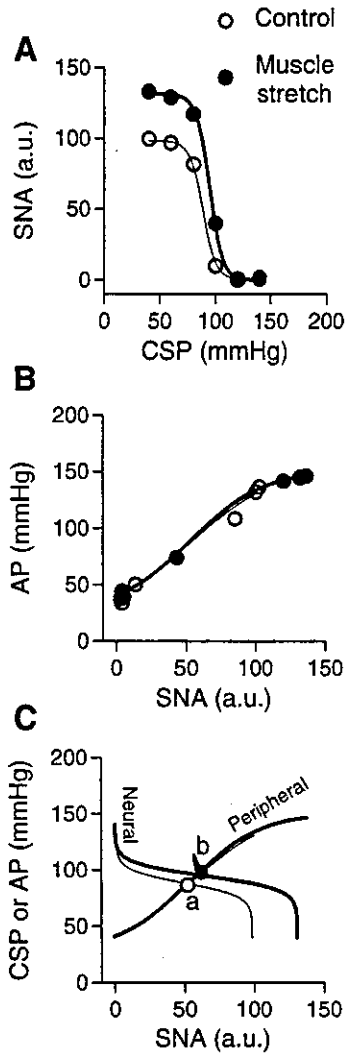

Fig. 3. Baroreflex neural arcs (*A*), peripheral arcs (*B*), and baroreflex equilibrium diagrams (*C*). In the neural (*A*) and peripheral arcs (*B*), the open and closed circles represent data points obtained under control and muscle stretch conditions, respectively. The thin and thick solid lines indicate fitted logistic functions under control and muscle stretch conditions, respectively. Muscle stretch increased SNA at CSP levels up to 100 mmHg in the neural arc. The peripheral arcs under both conditions were nearly identical. In baroreflex equilibrium diagrams (*C*), the thin and thick solid lines indicate fitted logistic functions under control and muscle stretch conditions, respectively. Because CSP is equilibrated with AP under physiological conditions, the operating point is determined from the intersection of the neural and peripheral arcs. Muscle stretch moved the operating point toward a higher AP (from *point a* to *point b*).

Figure 4*A* illustrates the role of the baroreflex function during muscle stretch and is derived from representative data from one animal. Muscle stretch almost doubled SNA from 54 to 98 au at the CSP level of the control operating point (*point a*), resulting in an elevation in AP of ~50%, from 87 to 130 mmHg (*point c*). When the arterial baroreflex was operative, the increases in SNA and AP recorded during muscle stretch were substantially attenuated (*point b*).

Figure 4*B* shows the group-averaged CSP, SNA, and AP obtained from eight animals under control and muscle stretch conditions at the CSP level of 93 ± 8 mmHg (control operating

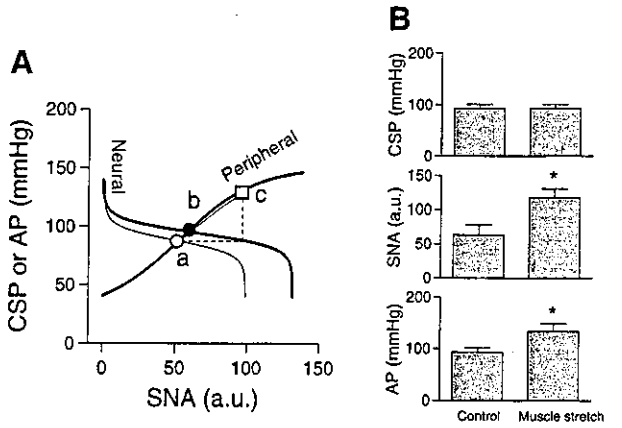

Fig. 4. *A*: role of the baroreflex function during muscle stretch derived from representative data from one animal. The thin and thick solid lines indicate the baroreflex equilibrium diagram under control and muscle stretch conditions, respectively. *Points a* and *b* represent the operating points under baseline and muscle stretch conditions, respectively. In instances where changes in AP during muscle stretch were not sensed by the arterial baroreflex, SNA would increase to ~100 au, resulting in elevation of AP above ~130 mmHg (*point c*). *B*: group-averaged CSP, SNA, and AP obtained from 8 animals under control and muscle stretch conditions at the CSP level of 93 ± 8 mmHg (control operating point). Muscle stretch nearly doubled the SNA, indicating that muscle stretch shifted the neural arc to SNA levels approximately twice at the CSP level of the control operating point. The twofold increase in SNA induced an AP elevation of ~50% at the same CSP level. *$P < 0.05$ from control.

point). Muscle stretch nearly doubled SNA, indicating that the muscle stretch shifted the neural arc to SNA values approximately twice those at the CSP level of the control operating point. This twofold increase in SNA induced an AP elevation of ~50% at the same CSP level.

The group-averaged parameters of the neural and peripheral arcs are summarized in Table 1. In the neural arc, the response range of SNA (P_1) and the midpoint of the operating range (P_3) were increased by muscle stretch. The coefficient of gain (P_2) and the minimum value of SNA (P_4) did not differ between control and muscle stretch conditions. G_{max} was increased by muscle stretch. In the peripheral arc, muscle stretch did not affect any of the four parameters or G_{max}. Muscle stretch significantly increased both AP and SNA at the operating point estimated from the baroreflex equilibrium diagram. A supplementary experiment associated with *protocol 2a* demonstrated that the effects of muscle stretch on the neural arc were abolished by tibial denervation (Table 2).

Table 1. *Effect of muscle stretch on the neural and peripheral arc parameters and operating point*

	Control	Muscle Stretch
Neural arc		
P_1, au	98.7±4.0	132.6±16.0*
P_2, au/mmHg	0.12±0.04	0.13±0.03
P_3, mmHg	104±11	109±11*
P_4, au	0.1±2.3	5.2±9.2
G_{max} au/mmHg	−2.9±0.9	−4.4±0.9*
Peripheral arc		
P_1, mmHg	118±30	118±10
P_2, au/mmHg	−0.05±0.02	−0.04±0.01
P_3, au	67.5±24.3	71.4±28.3
P_4, mmHg	30±11	34±7
G_{max}, au/mmHg	1.3±0.3	1.3±0.4
Values at operating point		
AP, mmHg	93±8	109±12*
SNA, au	63.1±15.1	81.2±21.0*

Values are means ± SD; $n = 8$ animals. See *Eq. 1* for definitions of the four parameters of logistic function (P_1–P_4). G_{max}, maximum gain. *$P < 0.05$ from control.

In *protocol 2b*, the actual operating point was measured by closing the baroreflex negative feedback loop. Muscle stretch increased AP from 92 ± 8 to 109 ± 14 mmHg ($P < 0.05$) and SNA from 61 ± 11 to 84 ± 25 au ($P < 0.05$) at the operating point. Figure 5 shows the relationship between the operating point estimated from the equilibrium diagram and that measured in eight animals. Each animal provided two data points determined under control and muscle stretch conditions (16 data points in total). For both AP and SNA, the estimated values were similar to the measured results. Root mean square errors of estimate were 4% for AP and 11% for SNA.

DISCUSSION

The key new findings of the present study are as follows. Muscle stretch reset the carotid sinus baroreflex neural arc to a higher SNA. In contrast, muscle stretch did not affect the baroreflex peripheral arc. As a result, the operating point determined from the intersection of the neural and peripheral arcs moved toward a higher AP during muscle stretch. These results support the hypothesis that the muscle mechanoreflex induces the pressor response by resetting the arterial baroreflex neural arc.

Interaction between the muscle mechanoreflex and arterial baroreflex. Although Potts and Li (31) showed that elevation of CSP attenuated the pressor response induced by muscle stretch, they did not measure SNA in that study. Our study demonstrated that the muscle mechanoreflex shifted the CSP-SNA curve toward a higher SNA primarily at low and midrange CSP readings (Fig. 3 and Table 1). This was not an outcome of the time-dependent changes in the muscle stretch effect, because the muscle stretch produced a sustained SNA increase for at least 7 min (Fig. 1). These results suggest that the baroreceptor input pressure-dependent pressor response due to muscle stretch is a consequence of the neural interaction between the muscle mechanoreflex and arterial baroreflex.

Miki et al. (26) demonstrated that treadmill exercise shifted the relationship between baroreceptor pressure input and SNA to a higher SNA. The shift in the baroreflex neural arc evoked by the muscle mechanoreflex may contribute to the exercise-induced resetting in the baroreflex control of SNA. Further-

Table 2. *Effect of muscle stretch after severing of the nerve supply to the hindlimb muscles on parameters of logistic function analysis for the neural arc*

	Control	Muscle Stretch
Neural arc		
P_1 au	99.5±2.1	100.8±8.2
P_2, au/mmHg	0.12±0.03	0.11±0.02
P_3, mmHg	107±5	110±8
P_4, au	0.3±1.6	0.2±3.7
G_{max}, au/mmHg	−2.9±0.7	−2.8±0.6

Values are means ± SD; $n = 5$ animals.

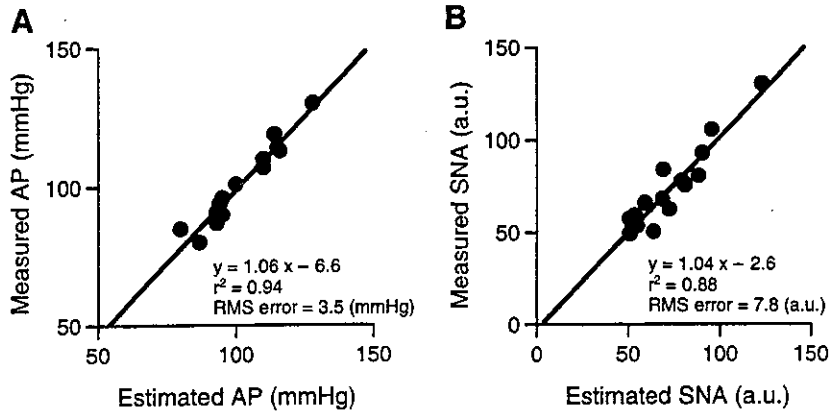

Fig. 5. Relationship between the operating point estimated from the equilibrium diagram and operating point actually measured in 8 animals. Each animal provided two data points determined under control and muscle stretch conditions (16 data points in total). The operating point estimated by the baroreflex equilibrium diagram matched the value obtained from actual measurements. *A*: measured vs. estimated AP; *B*: measured vs. estimated SNA. RMS, root mean square.

more, G_{max} of the neural arc (the CSP-SNA relationship) was increased by muscle stretch when the data were analyzed using a fitted logistic function (*Eq. 1*). The present result is consistent with previous studies (14, 26) showing that gain in the arterial baroreflex control of vascular sympathetic outflow was increased during static and dynamic exercise. On the other hand, another study showed no changes in the gain of the carotid sinus baroreflex control of SNA during dynamic arm exercise (5). Whether changes in the neural arc gain depend on the intensity and/or modality of exercise awaits further studies.

Previous studies (1, 40) suggest interactions between the muscle mechanoreflex and the arterial baroreflex in the brain stem. Baroreceptor afferent inputs inhibit neurons in the rostral ventrolateral medulla (RVLM). Electrically induced muscle contraction increases the firing frequency in RVLM neurons (2, 3), suggesting that the baroreflex and muscle mechanoreflex share common central pathways. In addition, the contraction-sensitive muscle afferents inhibit the baroreflex signal transduction through activation of GABA receptors in the nucleus tractus solitarii (33). This neural integration in the brainstem may be involved in the resetting of the arterial baroreflex neural arc induced by the muscle mechanoreflex.

Determination of the operating point of the arterial baroreflex. SNA and AP during muscle stretch may be determined via interactions between the muscle mechanoreflex and the arterial baroreflex. Muscle stretch shifted the neural arc to SNA values approximately double at the CSP level derived from the control operating point, whereas it did not affect the peripheral arc (Table 1 and Figs. 3 and 4). As a result, the operating point derived from the intersection of the two arcs moved toward a higher AP (Fig. 3*C*). These findings suggest that resetting in the neural arc, rather than in the peripheral arc, is responsible for the increases in SNA and AP during muscle stretch observed under baroreflex closed-loop conditions (21, 41). These data are the first to provide quantitative evidence demonstrating that resetting of the carotid sinus baroreflex (via central resetting of the baroreflex neural arc) is necessary to evoke the sympathoexcitatory and pressor responses associated with activation of mechanosensitive afferents in the closed-loop conditions.

The baroreflex equilibrium diagram is useful for intuitive understanding of the cardiovascular controls (28, 38). Figure 4*A* illustrates the role of the baroreflex function during muscle stretch. The baseline operating point was determined from the intersection of the neural and peripheral arcs (*point a*). Muscle stretch reset the neural arc from the thin line to the thick line. If changes in AP were not sensed by the arterial baroreflex, then muscle stretch nearly doubled SNA, resulting in AP elevation above ~130 mmHg (*point c*). However, when the arterial baroreflex was operative, the increases in SNA and AP during the muscle stretch were substantially attenuated (*point b*).

Sato et al. (38) demonstrated that the actual operating point matched the intersection of the neural and peripheral arcs under both control and hemorrhagic conditions. In the present study, the operating point estimated from the equilibrium diagram was in close agreement with that actually measured under both control and muscle stretch conditions (Fig. 5). These results confirm the accuracy of the operating point estimation derived from the equilibrium diagram.

Physiological implications. Dynamic exercise causes only a modest rise in mean AP despite a marked sympathoexcitation (36). This phenomenon is believed to be a consequence of the decreased sympathetic constrictor response due to metabolic vasodilation and sympatholysis in exercising muscles (4, 11, 12, 37). Figure 6 illustrates a putative diagram of the arterial baroreflex control of SNA and AP during the dynamic exercise. The muscle mechanoreflex resets the neural arc to a higher SNA. Vasodilation in exercising muscles presumably shifts the peripheral arc downward. If the neural arc is not reset to a higher SNA during dynamic exercise, AP at the operating point might decrease (*point c*) relative to that observed under resting conditions (*point a*). However, by resetting the neural

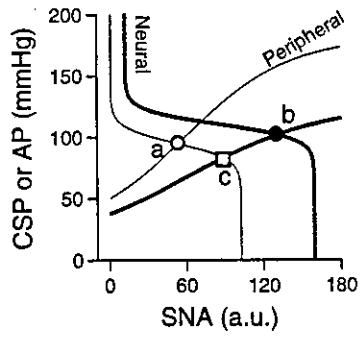

Fig. 6. Putative diagram of the arterial baroreflex controls of SNA and AP during dynamic exercise. Thin solid lines indicate the baroreflex equilibrium diagram under resting conditions. Thick solid lines indicate the baroreflex equilibrium diagram during dynamic exercise. *Points a* and *b* represent the operating points at rest and during exercise, respectively. If the neural arc did not reset to a higher SNA during dynamic exercise, then AP at the operating point would decrease (*point c*).

arc, AP may be maintained against the downward shift in the peripheral arc (*point b*). Thus we speculate that resetting of the neural arc induced by the muscle mechanoreflex contributes to maintaining AP despite the downward shift of the peripheral arc due to vasodilation in exercising muscles.

In the present study, we did not examine additional factors that may potentially influence SNA and AP regulation such as central command, muscle metaboreflex, and vasodilation in exercising muscles. Further investigations are required to improve our understanding of the arterial baroreflex control of SNA and AP during exercise.

Limitations. The present study has several limitations. First, we performed the experiment in animals under anesthetized conditions. Although anesthesia was convenient for elimination of the central command, the gain of carotid baroreflex and muscle mechanoreflex might have been estimated differently if the animals had been conscious.

Second, we used passive muscle stretch as the input for the muscle mechanoreflex. The shift in the baroreflex neural arc was abolished by the tibial denervation (Table 2), suggesting that the shift was evoked by the neural afferents from hindlimb muscles. Previous studies (10, 25, 39) have suggested that passive muscle stretch selectively activates muscle mechanoreceptors. Thus we believe that muscle stretch had evoked the muscle mechanoreflex in the present study.

In conclusion, the muscle mechanoreflex resets the arterial baroreflex neural arc to a higher SNA. Consequently, the pressor response is evoked during muscle stretch under baroreflex closed-loop conditions. This shift in the neural arc induced by the muscle mechanoreflex might compensate for AP falls resulting from exercise-induced vasodilatation.

GRANTS

This study was supported by Ministry of Health Labour and Welfare of Japan Health and Labour Sciences Research Grant for Research on Advanced Medical Technology 13090401 (H14-Nano-002), by Japan Society for the Promotion of Science Grant-in-Aid for Scientific Research (A) 15200040, and by the Program for Promotion of Fundamental Studies in Health Science of the Organization for Pharmaceutical Safety and Research of Japan.

REFERENCES

1. **Aicher SA, Kurucz OS, Reis DJ, and Milner TA.** Nucleus tractus solitarius efferent terminals synapse on neurons in the caudal ventrolateral medulla that project to the rostral ventrolateral medulla. *Brain Res* 693: 51–63, 1995.
2. **Bauer RM, Iwamoto GA, and Waldrop TG.** Discharge patterns of ventrolateral medullary neurons during muscular contraction. *Am J Physiol Regul Integr Comp Physiol* 259: R606–R611, 1990.
3. **Bauer RM, Waldrop TG, Iwamoto GA, and Holzwarth MA.** Properties of ventrolateral medullary neurons that respond to muscular contraction. *Brain Res Bull* 28: 167–178, 1992.
4. **Buckwalter JB, Naik JS, Valic Z, and Clifford PS.** Exercise attenuates α-adrenergic receptor responsiveness in skeletal muscle vasculature. *J Appl Physiol* 90: 172–178, 2001.
5. **Fadel PJ, Ogoh S, Watenpaugh DE, Wasmund W, Olivencia-Yurvati A, Smith ML, and Raven PB.** Carotid baroreflex regulation of sympathetic nerve activity during dynamic exercise in humans. *Am J Physiol Heart Circ Physiol* 280: H1383–H1390, 2001.
6. **Gallagher KM, Fadel PJ, Smith SA, Norton KH, Querry RG, Olivencia-Yurvati A, and Raven PB.** Increases in intramuscular pressure raise arterial blood pressure during dynamic exercise. *J Appl Physiol* 91: 2351–2358, 2001.
7. **Gallagher KM, Fadel PJ, Stromstad M, Ide K, Smith SA, Querry RG, Raven PB, and Secher NH.** Effects of exercise pressor reflex activation on carotid baroreflex function during exercise in humans. *J Physiol* 533: 871–880, 2001.
8. **Gallagher KM, Fadel PJ, Stromstad M, Ide K, Smith SA, Querry RG, Raven PB, and Secher NH.** Effects of partial neuromuscular blockade on carotid baroreflex function during exercise in humans. *J Physiol* 533: 861–870, 2001.
9. **Hayes SG and Kaufman MP.** Gadolinium attenuates exercise pressor reflex in cats. *Am J Physiol Heart Circ Physiol* 280: H2153–H2161, 2001.
10. **Hayes SG and Kaufman MP.** MLR stimulation and exercise pressor reflex activate different renal sympathetic fibers in decerebrate cats. *J Appl Physiol* 92: 1628–1634, 2002.
11. **Howard MG and DiCarlo SE.** Reduced vascular responsiveness after a single bout of dynamic exercise in the conscious rabbit. *J Appl Physiol* 73: 2662–2667, 1992.
12. **Howard MG, DiCarlo SE, and Stallone JN.** Acute exercise attenuates phenylephrine-induced contraction of rabbit isolated aortic rings. *Med Sci Sports Exerc* 24: 1102–1107, 1992.
13. **Iellamo F, Legramante JM, Raimondi G, and Peruzzi G.** Baroreflex control of sinus node during dynamic exercise in humans: effects of central command and muscle reflexes. *Am J Physiol Heart Circ Physiol* 272: H1157–H1164, 1997.
14. **Kamiya A, Michikami D, Fu Q, Niimi Y, Iwase S, Mano T, and Suzumura A.** Static handgrip exercise modifies arterial baroreflex control of vascular sympathetic outflow in humans. *Am J Physiol Regul Integr Comp Physiol* 281: R1134–R1139, 2001.
15. **Kaufman MP and Forster HV.** Reflexes controlling circulatory, ventilatory and airway responses to exercise. In: *Handbook of Physiology. Exercise: Regulation and Integration of Multiple Systems. Control of Respiratory and Cardiovascular Systems.* Bethesda, MD: Am. Physiol. Soc., 1996, sect. 12, pt. II, chapt. 10, p. 381–447.
16. **Kawada T, Shishido T, Inagaki M, Tatewaki T, Zheng C, Yanagiya Y, Sugimachi M, and Sunagawa K.** Differential dynamic baroreflex regulation of cardiac and renal sympathetic nerve activities. *Am J Physiol Heart Circ Physiol* 280: H1581–H1590, 2001.
17. **Kawada T, Shishido T, Inagaki M, Zheng C, Yanagiya Y, Uemura K, Sugimachi M, and Sunagawa K.** Estimation of baroreflex gain using a baroreflex equilibrium diagram. *Jpn J Physiol* 52: 21–29, 2002.
18. **Kawada T, Uemura K, Kashihara K, Jin Y, Li M, Zheng C, Sugimachi M, and Sunagawa K.** Uniformity in dynamic baroreflex regulation of left and right cardiac sympathetic nerve activities. *Am J Physiol Regul Integr Comp Physiol* 284: R1506–R1512, 2003.
19. **Kent BB, Drane JW, Blumenstein B, and Manning JW.** A mathematical model to assess changes in the baroreceptor reflex. *Cardiology* 57: 295–310, 1972.
20. **Leshnower BG, Potts JT, Garry MG, and Mitchell JH.** Reflex cardiovascular responses evoked by selective activation of skeletal muscle ergoreceptors. *J Appl Physiol* 90: 308–316, 2001.
21. **Matsukawa K, Wall PT, Wilson LB, and Mitchell JH.** Reflex responses of renal nerve activity during isometric muscle contraction in cats. *Am J Physiol Heart Circ Physiol* 259: H1380–H1388, 1990.
22. **McCloskey DI and Mitchell JH.** Reflex cardiovascular and respiratory responses originating in exercising muscle. *J Physiol* 224: 173–186, 1972.
23. **McIlveen SA, Hayes SG, and Kaufman MP.** Both central command and exercise pressor reflex reset carotid sinus baroreflex. *Am J Physiol Heart Circ Physiol* 280: H1454–H1463, 2001.
24. **Melcher A and Donald DE.** Maintained ability of carotid baroreflex to regulate arterial pressure during exercise. *Am J Physiol Heart Circ Physiol* 241: H838–H849, 1981.
25. **Mense S and Stahnke M.** Responses in muscle afferent fibres of slow conduction velocity to contractions and ischaemia in the cat. *J Physiol* 342: 383–397, 1983.
26. **Miki K, Yoshimoto M, and Tanimizu M.** Acute shifts of baroreflex control of renal sympathetic nerve activity induced by treadmill exercise in rats. *J Physiol* 548: 313–322, 2003.
27. **Mitchell JH, Kaufman MP, and Iwamoto GA.** The exercise pressor reflex: its cardiovascular effects, afferent mechanisms, and central pathways. *Annu Rev Physiol* 45: 229–242, 1983.
28. **Mohrman DE and Heller LJ.** *Cardiovascular Physiology* (4th ed.). New York: McGraw-Hill, 1997, p. 158–230.
29. **Norton KH, Boushel R, Strange S, Saltin B, and Raven PB.** Resetting of the carotid arterial baroreflex during dynamic exercise in humans. *J Appl Physiol* 87: 332–338, 1999.
30. **Papelier Y, Escourrou P, Gauthier JP, and Rowell LB.** Carotid baroreflex control of blood pressure and heart rate in men during dynamic exercise. *J Appl Physiol* 77: 502–506, 1994.

31. **Potts JT and Li J.** Interaction between carotid baroreflex and exercise pressor reflex depends on baroreceptor afferent input. *Am J Physiol Heart Circ Physiol* 274: H1841–H1847, 1998.
32. **Potts JT and Mitchell JH.** Rapid resetting of carotid baroreceptor reflex by afferent input from skeletal muscle receptors. *Am J Physiol Heart Circ Physiol* 275: H2000–H2008, 1998.
33. **Potts JT, Paton JF, Mitchell JH, Garry MG, Kline G, Anguelov PT, and Lee SM.** Contraction-sensitive skeletal muscle afferents inhibit arterial baroreceptor signalling in the nucleus of the solitary tract: role of intrinsic GABA interneurons. *Neuroscience* 119: 201–214, 2003.
34. **Potts JT, Shi XR, and Raven PB.** Carotid baroreflex responsiveness during dynamic exercise in humans. *Am J Physiol Heart Circ Physiol* 265: H1928–H1938, 1993.
35. **Rowell LB and O'Leary DS.** Reflex control of the circulation during exercise: chemoreflexes and mechanoreflexes. *J Appl Physiol* 69: 407–418, 1990.
36. **Rowell LB, O'Leary DS, and Kellogg DS.** Integration of cardiovascular control system in dynamic exercise. In: *Handbook of Physiology. Exercise: Regulation and Integration of Multiple Systems.* Bethesda, MD: Am. Physiol. Soc., sect. 12, pt. II, chapt. 17, 1996, p. 770–838.
37. **Ruble SB, Valic Z, Buckwalter JB, and Clifford PS.** Dynamic exercise attenuates sympathetic responsiveness of canine vascular smooth muscle. *J Appl Physiol* 89: 2294–2299, 2000.
38. **Sato T, Kawada T, Inagaki M, Shishido T, Takaki H, Sugimachi M, and Sunagawa K.** New analytic framework for understanding sympathetic baroreflex control of arterial pressure. *Am J Physiol Heart Circ Physiol* 276: H2251–H2261, 1999.
39. **Stebbins CL, Brown B, Levin D, and Longhurst JC.** Reflex effect of skeletal muscle mechanoreceptor stimulation on the cardiovascular system. *J Appl Physiol* 65: 1539–1547, 1988.
40. **Sun MK and Guyenet PG.** GABA-mediated baroreceptor inhibition of reticulospinal neurons. *Am J Physiol Regul Integr Comp Physiol* 249: R672–R680, 1985.
41. **Victor RG, Rotto DM, Pryor SL, and Kaufman MP.** Stimulation of renal sympathetic activity by static contraction: evidence for mechanoreceptor-induced reflexes from skeletal muscle. *Circ Res* 64: 592–599, 1989.
42. **Waldrop TG, Eldridge FL, Iwamoto GA, and Mitchell JH.** Central neural control of respiration and circulation during exercise. In: *Handbook of Physiology. Exercise: Regulation and Integration of Multiple Systems. Control of Respiratory and Cardiovascular Systems.* Bethesda, MD: Am. Physiol. Soc., 1996, sect. 12, pt. II, chapt. 9, p. 333–380.

Excessive Increase in QT Interval and Dispersion of Repolarization Predict Recurrent Ventricular Tachyarrhythmia after Amiodarone

TAKESHI AIBA,*† WATARU SHIMIZU,* MASASHI INAGAKI,† KAZUHIRO SATOMI,* ATSUSHI TAGUCHI,* TAKASHI KURITA,* KAZUHIRO SUYAMA,* NAOHIKO AIHARA,* KENJI SUNAGAWA,† and SHIRO KAMAKURA*

From the *Division of Cardiology, Department of Internal Medicine, and the †Department of Cardiovascular Dynamics, Research Institute, National Cardiovascular Center, Suita, Japan

AIBA, T., ET AL.: Excessive Increase in QT Interval and Dispersion of Repolarization Predict Recurrent Ventricular Tachyarrhythmia after Amiodarone. *Although chronic amiodarone has been proven to be effective to suppress ventricular tachycardia (VT) and ventricular fibrillation (VF), how we predict the recurrence of VT/VF after chronic amiodarone remains unknown. This study evaluated the predictive value of the QT interval, spatial, and transmural dispersions of repolarization (SDR and TDR) for further arrhythmic events after chronic amiodarone. Eighty-seven leads body surface ECGs were recorded before (pre) and one month after (post) chronic oral amiodarone in 50 patients with sustained monomorphic VT associated with organic heart disease. The Q-Tend (QTe), the Q-Tpeak (QTp), and the interval between Tpeak and Tend (Tp-e) as an index of TDR were measured automatically from 87-lead ECG, corrected Bazett's method (QTce, QTcp, Tcp-e), and averaged among all 87 leads. As an index of SDR, the maximum (max) minus minimum (min) QTce (max-min QTce) and standard deviation of QTce (SD-QTce) was obtained among 87 leads. All patients were prospectively followed (15 ± 10 months) after starting amiodarone, and 20 patients had arrhythmic events. The univariate analysis revealed that post max QTce, post SD-QTce, post max-min QTce, and post mean Tcp-e from 87-lead but not from 12-lead ECG were the significant predictors for further arrhythmic events. ROC analysis indicated the post max-min QTce ≥106 ms as the best predictor of events (hazard ratio = 10.4, 95%, CI 2.7 to 40.5, P = 0.0008). Excessive QT prolongation associated with increased spatial and transmural dispersions of repolarization predict the recurrence of VT/VF after amiodarone treatment. (PACE 2004; 27:901–909)*

amiodarone, QT interval, dispersion, ventricular tachycardia, prognosis

Introduction

Spatial heterogeneity of ventricular repolarization has been important as the genesis of ventricular tachyarrhythmias.[1] The QT dispersion and recovery time dispersion, which are assumed to reflect the spatial heterogeneity,[2,3] have been proposed as a marker of electrical instability under several conditions, such as congenital long QT syndrome (LQTS).[4–9] On the other hand, recent experimental studies have suggested that transmural dispersion of repolarization (TDR) across the ventricular wall (epicardial, midmyocardial (M), and endocardial cells) was linked to ventricular arrhythmias such as torsades de pointes (TdP) under LQTS conditions.[10–12] The peak and the end of the T wave in the ECG are reported to coincide with repolarization of the epicardial and the longest M cell action potentials, respectively,[13] so that the interval between the Tpeak and Tend (Tp-e) is expected to reflect TDR.[14,15]

Chronic amiodarone therapy reduced slowly activating delayed rectifier K^+ currents (I_{Ks}) in the ventricular myocardium,[16] resulting in prolongation of action potential duration and suppression of life-threatening tachyarrhythmia in patients with structural heart disease.[17] Although amiodarone is classified into Class III antiarrhythmic agents, TdP is rare due to homogeneous prolongation of regional ventricular repolarization (QT interval).[18,19] Previous studies have attempted to show the effect of amiodarone on the QT interval and QT dispersion in the standard 12-lead electrocardiogram (ECG).[20–22] However, the change of QT dispersion after amiodarone therapy was

Dr. Shimizu was supported in part by the Japanese Cardiovascular Research Foundation, Vehicle Racing Commemorative Foundation, and Health Sciences Research Grants from the Ministry of Health, Labor and Welfare, and Research Grant for Cardiovascular Diseases (15C-6) from the Ministry of Health, Labor and Welfare, Japan.

Presented in part at the 24th North American Society of Pacing and Electrophysiology (NASPE) meeting, Washington DC, May 14, 2003, and published as an abstract (PACE 2003; 26:998).

Wataru Shimizu, M.D., Division of Cardiology, Department of Internal Medicine, National Cardiovascular Center, 5-7-1 Fujishiro-dai, Suita, Osaka, 565-8565 Japan. Fax: 81-6-6872-7486; e-mail: wshimizu@hsp.ncvc.go.jp

Received August 12, 2003; revised February 19, 2004; accepted March 2, 2004.

controversial. Moreover, the effect of amiodarone therapy on TDR was reported only in some experimental studies,[23–25] but not in a clinical study. In the present study, we measured the spatial and transmural dispersions of repolarization obtained from the 87-lead body surface mapping ECG before and 1 month after starting oral amiodarone, and investigated the predictive value of these repolarization parameters for recurrence of ventricular tachyarrhythmias. Our results suggested that excessive prolongation of the maximum QTc interval associated with increased spatial and transmural dispersions of repolarization predicted the risk of further arrhythmic events after amiodarone.

Methods

Patient Population

We prospectively investigated 50 patients (39 men, 11 women) with a mean age of 57 ± 10 years (Table I), who had been referred to the National Cardiovascular Center between 1993 and 2001. All patients had a history of symptomatic sustained monomorphic ventricular tachycardia (VT) associated with prior myocardial infarction (22 patients), dilated cardiomyopathy (21 patients), and arrhythmogenic right ventricular cardiomyopathy (7 patients). Mean left ventricular ejection fraction (LVEF) was 31% ± 12%, and 47 (94%) patients were in New York Heart Association functional class (NYHA) I or II. All patients were in sinus rhythm, and had no complete right or left bundle branch block. They received oral amiodarone with loading dose of 300 or 400 mg/day for two weeks followed by maintenance dose of 150 or 200 mg/day. Dose or type of β-blockers, angiotensin converting enzyme inhibitor, and other cardiac active drugs were not changed in all patients during the follow-up periods. The other antiarrhythmic medications were discontinued for at least five drug half-lives before administration of oral amiodarone. The median follow-up periods before amiodarone treatment were 5 months (1-156 months) and the incidence of pretreatment VT was 0.50 times (0.06-2.0)/month. The protocol of this study was explained to all patients, and informed consent was obtained from all patients.

Table I.

Patients Characteristics

Patients (n)	50
Age (yrs)	57 (10)
Gender (Men)	39
Basal disease (n)	
prior MI	22
DCM	21
ARVC	7
NYHA (I/II/III)	19/28/3
LVEF (%)	31 (12)
VT rate (/min)	188 (29)
Medication [n (%)]	
ACE-I	23 (46%)
β-blocker	17 (34%)
digitalis	14 (28%)
ICD (%)	15 (30%)

The data of Age, LVEF, and VT rate are presented as the mean value (SD).
ACE-I = angiotensin converting enzyme inhibitor; ARVC = arrhythmogenic right ventricular cardiomyopathy; DCM = dilated cardiomyopathy; LVEF = left ventricular ejection fraction; MI = myocardial infarction; NYHA = New York Heart Association functional class; VT = ventricular tachycardia.

Measurements of the 87-Lead Body Surface ECG

Eighty-seven-lead body surface ECG and standard 12-lead ECG were simultaneously recorded with a VCM-3000 (Fukuda Denshi Co., Tokyo, Japan) before (pre) and 1 month after (post) starting oral amiodarone in all patients. The method for recording have been detailed in previous studies.[8,14,15] These ECG data were simultaneously digitized at 1.0 kHz in each channel, stored on a floppy disk, and transferred to a personal computer with the analysis program developed by our institution. The 87-lead and 12-lead ECGs were analyzed using an automatic digitized program. The Q-Tend interval (QTe) was defined as the time interval between the QRS onset and the point at which the isoelectric line intersected a tangential line drawn at the minimum first derivative (dV/dt) point of the positive T wave or at the maximum dV/dt point of the negative T wave. When a bifurcated or secondary T wave (pathological U wave) appeared, it was included as part of the measurement of the QT interval, but a normal U wave, which was apparently separated from T wave, was not included. The Q-Tpeak interval (QTp) was defined as the time interval between the QRS onset and the point at the peak of positive T wave or the nadir of the negative T wave. When a T wave had a biphasic or a notched configuration, peak of the T wave was defined as that of the dominant T wave deflection. If the end and peak of the T wave was unidentifiable because of the flat or low amplitude T wave (amplitude < 0.05 mV), the lead was excluded. The QTe, the QTp, as well as the Tp-e (QTe minus QTp) as an index of TDR were measured automatically from all 87-lead ECGs, corrected to heart rate by Bazett's method (QTce, QTcp, Tcp-e: QTe/$\sqrt{RR}$, QTp/$\sqrt{RR}$, Tp-e/$\sqrt{RR}$), and averaged among 87 leads. Each point determined by the computer was checked visually for each lead. As an index of spatial dispersion of repolarization (SDR), the maximum